Federal Agency:	Department of Energy
FOA Name:	FY 2013 Vehicle Technologies Program
FOA Number:	DE-FOA-0000793
Award Number:	DE-EE0006437
Prime Recipient:	Daikin America, Inc.
Project Title:	Daikin Advanced Lithium Ion Battery Technology – High Voltage Electrolyte
Principal Investigator:	Joe Sunstrom, Ron Hendershot
Team Members:	Michael Gilmore, Hitomi Miyawaki, Akiyoshi Yamauchi, Abundio Sandoval, Teresa Stewart
Date:	February 8, 2017
Period Covered:	Final Report: October, 2013 – September, 2016

Executive Summary

An evaluation of high voltage electrolytes which contain fluorochemicals as solvents/additive has been completed with the objective of formulating a safe, stable electrolyte capable of operation to 4.6 V. Stable cycle performance has been demonstrated in $LiNi_{1/3}Mn_{1/3}Co_{1/3}O_2$ (NMC111)/graphite cells to 4.5 V. The ability to operate at high voltage results in significant energy density gain (>30%) which would manifest as longer battery life resulting in higher range for electric vehicles. Alternatively, a higher energy density battery can be made smaller without sacrificing existing energy. In addition, the fluorinated electrolytes examined showed better safety performance when tested in abuse conditions. The results are promising for future advanced battery development for vehicles as well as other applications.

Milestone	Type	Description	Status
Complete Identification of Promising Electrolyte Formulations	Technical	Experimental design completed with consistent data sufficient to build models. Promising electrolyte formulations are identified which are suitable for high-voltage battery testing.	Completed
Fabrication and Delivery of Interim Cells	Technical	Successful fabrication of 10 interim cells and delivery of cells to DOE laboratory to be specified.	Completed
Demonstrate Stable Performance at 4.6 volts	Go/No Go	Electrochemical and battery cycle tests are completed and promising results are obtained which demonstrate stable performance at 4.6 volts	Completed Test result 100 cycles at 4.6 V - Go
Confirm Final Electrolyte Formulations	Technical	Confirm correlations of battery tests, surface analysis compositional analysis, and electrochemical results and use the complete data set to identify best performing electrolyte compositions.	Completed
Fabrication and Delivery of Final Cells	Technical	Successful fabrication of 10 improved cells and delivery of cells to DOE laboratory to be specified. Cell test plans, cell design, and cell performance and abuse test documentation is completed.	30 cells have been delivered for evaluation at 4.5 and 4.6 V

Introduction

The capability of lithium ion batteries to play an increasing role in emerging technologies such as electric vehicles, advanced consumer devices, and stationary storage is predicated on the development of higher energy cells thus enabling longer usage cycles.[1] There are generally three routes to increasing the energy in these cells: selection of higher capacity materials, improved engineering of cells and higher voltage operation. Higher capacity battery materials particularly cathodes have been extensively studied.[2-3] Improved engineering is achieved through various routes such as thicker electrodes, reduction of non-actives and rebalance of cathode/anode ratios with the introduction of higher capacity actives. This study is focused on the third route to higher energy cells which is the ability to operate cells at high voltage.

The current state of the art lithium ion battery electrolyte is a mix of conventional hydrocarbon solvents, SEI (solid electrolyte interface) forming additives, gassing inhibitors and salt. Conventional hydrocarbon electrolytes are appropriate for voltages of less than 4.35 V vs. graphite. Consequently, the majority of cells on the commercial lithium ion market are targeted for performance at 4.2 V although at this writing there are several higher voltage options (> 4.2 V). At higher voltages, one noted failure mechanism is the decomposition of the liquid electrolyte leading to gassing in the cell.[4-12]

For liquid electrolytes, high stability ionic liquids[13] have been proposed as alternatives but exhibit high viscosity and lower conductivity due to the high molecular weight of the molecules. A more attractive solution is to develop electrolytes containing small molecules which have increased stability due to high bond strength.

Fluorocarbons are good examples of molecules which have high stability while still exhibiting acceptable physical properties for electrolytes. Figure 1 show calculated results for three common materials used in commercial battery electrolytes (left side) as compared with their fluorinated analogs (right side). The net effect of replacement of carbon-hydrogen bonds with carbon-fluorine bonds is to drop the energy of the Highest Occupied Molecular Orbital (HOMO) thus making the compound more stable to oxidation.

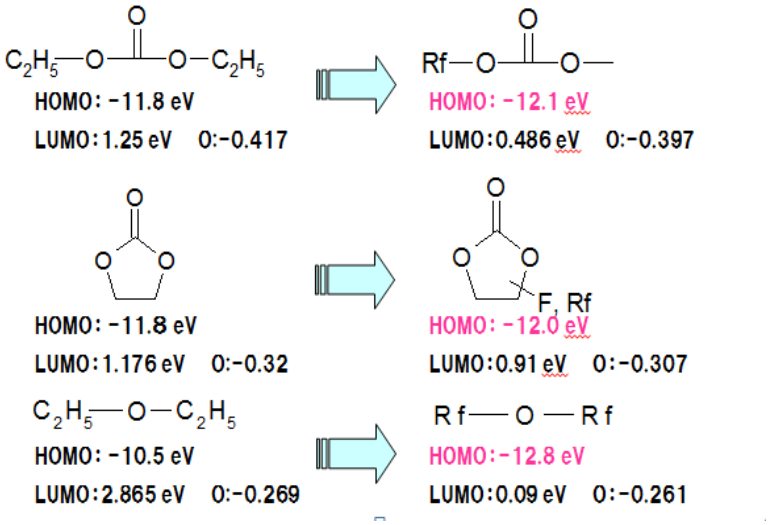

Figure 1 Theoretical calculation of the energies of the highest occupied molecular orbital (HOMO) and lowest unoccupied molecular orbital (LUMO) for some standard lithium ion electrolyte materials (left) and their fluorinated analogs (right)

This is verified experimentally in Figure 2 which shows the linear scanning voltammetry data for several examples of fluorocarbon and hydrocarbon based battery solvents. This experiment is completed using platinum electrode with a lithium metal reference. The fluorinated solvents show higher stability to voltage both at the onset point where current is first detected and catastrophic decomposition marked by fast current increase. Another experimental example of stable fluorinated electrolytes can be displayed in a floating point test. For this test shown in Figure 3, a piece of $LiNi_{0.33}Mn_{0.33}Co_{0.33}O_2$ cathode is placed into a flooded electrolyte cell and held at constant voltage. The decomposition current is then monitored. The ideal condition is for the decomposition current to go to zero as quickly as possible. In Figure 3, the electrolytes which are primarily hydrocarbon (blue and black traces) continue to pass current out to 4000 minutes. Practically, this means that these electrolytes could not be used in batteries which are stored in a charged state (4.6 V). The remaining electrolytes which contain a maximum of 10% fluorocarbon achieve no decomposition at much earlier times.

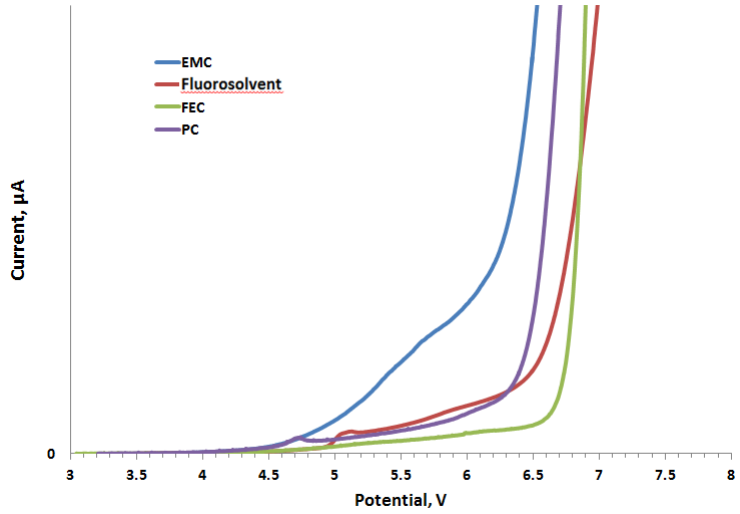

Figure 2 Linear scanning voltammetry scans of hydrocarbon (PC, EMC) and fluorocarbon (FEC, fluorosolvent) electrolyte solvents

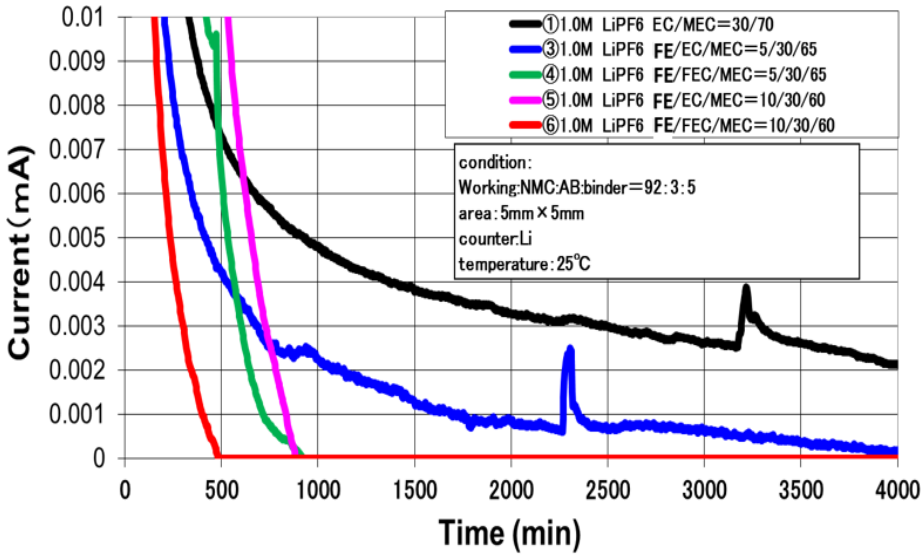

Figure 3 Floating point test of NMC111 cathode at 4.6 V for various hydrocarbon and fluorocarbon electrolytes

Safe operation of lithium ion batteries particularly high energy density batteries is another topic of high interest particularly (but not limited to) for consumer applications such as transportation and electronics.[14] Lithium ion batteries contain the three necessary elements for combustion: highly delithiated cathode (oxidizer), flammable electrolyte (fuel) and spark, heat (ignition source). There are

several strategies which involve removing one of the combustion elements. Selection of cathode materials which when de-lithiated are more stable and less oxidizing is one route to safer batteries, however, this often results in lower energy density. A second method involves engineering controls to minimize spark/heat exposure or for containment in the event of an exothermic event. A more straightforward approach to fire safety in lithium ion batteries is to lower/remove flammability of the electrolyte through prudent choice of chemistry.

There has been significant research into fluorochemicals as electrolyte components both external[15] and internal[16-21] to Daikin. The primary focus of using fluorinated electrolyte has been to enable high voltage cycling, increased high temperature stability and improved safety performance. A significant body of work has been accomplished looking at fluorochemistry as an alternative to 5 V batteries.[22-25] An example of internal commercial investigation of fluorinated electrolytes is shown in Figure 4. The target was to develop an electrolyte to cycle at 4.35 V which is near the voltage limit of commercially available cells. An explanation for this voltage limit can be noted in this data. The data shows 4.35 V 60 C cycling data which includes

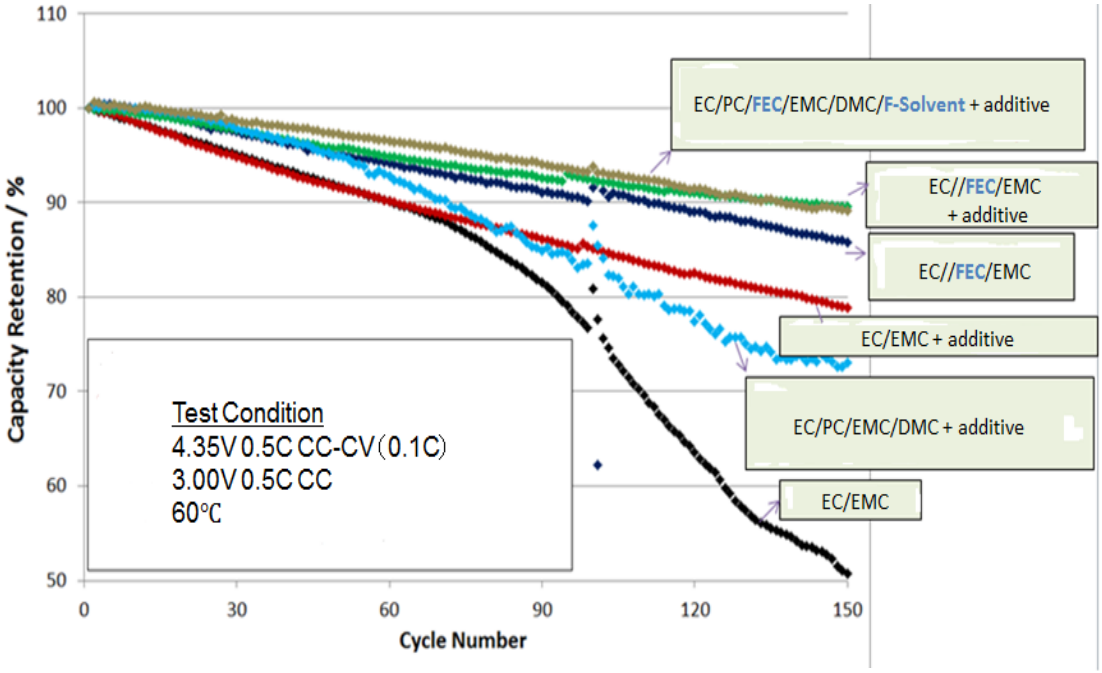

Figure 4 Accelerated (60 C) cycle life at 4.35 V for several fluorinated electrolytes (top four traces) compared to hydrocarbon controls (bottom two traces)

a hydrocarbon control (EC/EMC) and the commercially available control electrolyte (EC/PC/EMC/DMC + additive). Remarkable improvement in the cycling performance is achieved by addition of fluoroethylene carbonate (FEC), fluorosolvents and additives. A significant portion of this improvement is due to reduction of gassing.

Successful implementation of fluorocarbon based electrolytes will increase the energy densities in existing battery chemistries by allowing them to cycle at voltages which are unattainable by conventional hydrocarbon electrolytes. In addition, fluorocarbon chemistries have the potential to increase safety performance of lithium ion batteries.

Experimental

Cell chemistry choice and fabrication efforts

Initially, the chemistry chosen for this study was $LiMn_{1.5}Ni_{0.5}O_4$ (LMNO)/graphite cells. Nanomyte SP-10 cathode powder was purchased from NEI Corporation. Mag D graphite was obtained from Nippon. Electrode coating and cell construction were completed at Coulometrics LLC (Chattanooga). 100 45 Ah single layered prismatic cells were fabricated for testing at 4.6 V and are shown in Figure 5. There were some problems with consistency of cycling test results which could not be attributed solely to electrolyte. Because the source of the inconstancies could not be identified it was decided to use commercially produced NMC/graphite cells as a test vehicle for improved reproducibility of results. $LiNi_{0.33}Mn_{0.33}Co_{0.33}O_2$ Dry (NMC111)/Graphite dry cells were ordered from LiFan (China). The cells have a wound prismatic construction, 1 Ah nominal capacity and have a cathode/anode balance suited for 4.2 V operation.

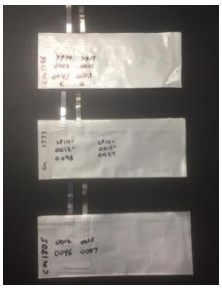

Figure 5 LMNO/graphite cells fabricated at Coulometrics.

Preparation of electrolytes

Battery grade lithium hexafluorophosphate ($LiPF_6$) was purchased from Kanto Denka. Battery grade ethylene carbonate(EC), ethyl methyl carbonate(EMC), dimethyl carbonate(DMC), and diethyl carbonate(DEC) were obtained from Kishida Chemical. Battery grade 1,3-Propane sultone (PS), vinylene carbonate (VC), and fluoroethylene carbonate (FEC) were ordered from Highchem America. Battery grade fluoroether, cyclic flourocarbonates, and fluorosulfonates were obtained from Daikin Industries, Ltd.(Japan). Solvents, salts, and additives were stored and mixed in an Inert Technology PL-HE-4BG-1800 glovebox with a controlled argon atmosphere with less than 5 ppm O_2 and H_2O.

Figure 6 In house cell for LSV measurements

When preparing samples for testing, the major solvent components of the electrolytes were mixed first by weight percent. After mixing solvents, the $LiPF_6$ was added to the solvent mixture. The solvent/salt mixture was allowed to sit overnight for complete salt dissolution and for the mixture to cool. Additives were then added to the solvent salt mixture.

Electrolyte conductivity measurements were made using a TOA-DKK CM-30R conductivity meter. Moisture analysis of both components and mixtures was complete using a KEM MXC-501 Karl Fischer Moisture Titrator. Gassing volume measurements were made using an Alfa Mirage MD300-S balance by the Archimedes method

Solvent and electrolyte stability was measured from 0-8 volts using a Princeton Applied Research VersaSTAT 4. An in-house test cell with both platinum and lithium electrodes is shown in Figure 6.

Cell Building and Formation

The dry cells were received sealed from the manufacturer. These cells were cut open then placed in a vacuum oven to dry at -30 in Hg and 60°C for at least 12 hours. The cells were then transferred immediately to the glovebox, where they were allowed to cool under vacuum in the glovebox antechamber. The dry weight of the cells was measured and recorded, and then electrolyte was added to the dry cells on a weight basis with the amount modified to account for the varying density of different electrolyte formulations. This ensured that equal volume of electrolyte was added to each cell. The cells were allowed to sit for 15 minutes to allow the electrolyte to soak into the electrode roll. The cells were then moved into the glovebox antechamber and placed under vacuum for 5 minutes to promote complete wetting of the electrode surfaces. The cells were allowed to sit for an additional 30 minutes after this vacuum treatment. Batteries were then transferred to an inert argon glove bag and sealed under vacuum using a Fuji Impulse FCB-200 vacuum sealer. The final weight of the cells was recorded after sealing was completed to determine the final amount of electrolyte within the cells. The cells were allowed to rest for 8 hours before formation cycling of the cells was performed. Cells were formed by cycling the cells at a rate of C/20 for two cycles.

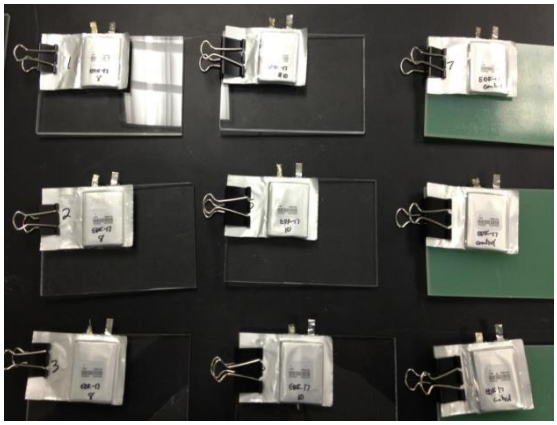

Figure 7 Finished 1 Ah NMC111/graphite cells

Cells were tested unclamped on Kikusui PFX 2011 battery channels at prescribed voltage, rate and temperature. Finished cells ready for testing are shown in Figure 7.

Thermal and abuse testing

Thermal analysis was performed using a TA Instruments Q500 Thermal Gravimetric Analyzer (TGA) and Q1000 Differential Scanning Calorimeter (DSC). Cells were charged to voltage of interest and transferred to the inert argon glovebox. The cells were then disassembled carefully to avoid electrically short of the cells. Electrodes were extracted wet with electrolyte and samples were obtained by scraping the electrode coating from the foil (< 15 mg sample). The samples were then immediately (< 5 mins) placed into hermetically sealed DSC pressure vessels. The pressure vessels were rated for 1000 psi maximum pressure. The sample and

reference pans were then placed into the DSC, allowed to equilibrate at 50 C, ramped 10 C/min to 350 and allowed to isothermal for 15 minutes. The experiment was run under nitrogen gas.

Results and Discussion

Electrolyte selection process

Choice of candidate electrolytes to complete this study was accomplished by a three step methodology which included:

1. Evaluation of physical properties of components (solvents, additives) as well as factors including cost and availability
2. Optimization of base solvent mixture through composition/physical property mapping.
3. Selection of additive package by a combination of charge counting techniques proposed by J. Dahn[26-30] as well as real time cycling measurements including gas evolution.

As a starting point, electrolytes of the following general formula were considered:

Solvents: Hydrocarbon(Fluorocarbon) A / Hydrocarbon B / Fluorocarbon C + *additives:* (D + E)

The solvent package contains a high permittivity solvent (A), a standard hydrocarbon solvent (B), and a standard fluorocarbon solvent (C) in that the volume percentages add to 100%. The mixture of hydrocarbon and fluorocarbon is proposed to maximize performance/cost ratio. The additive package (D + E) contains additives which have a variety of roles such as film formation (SEI layers) and gas mediation and are not restricted to solely fluorochemicals.

Table I. Solvent and additive combinations for electrolyte optimization

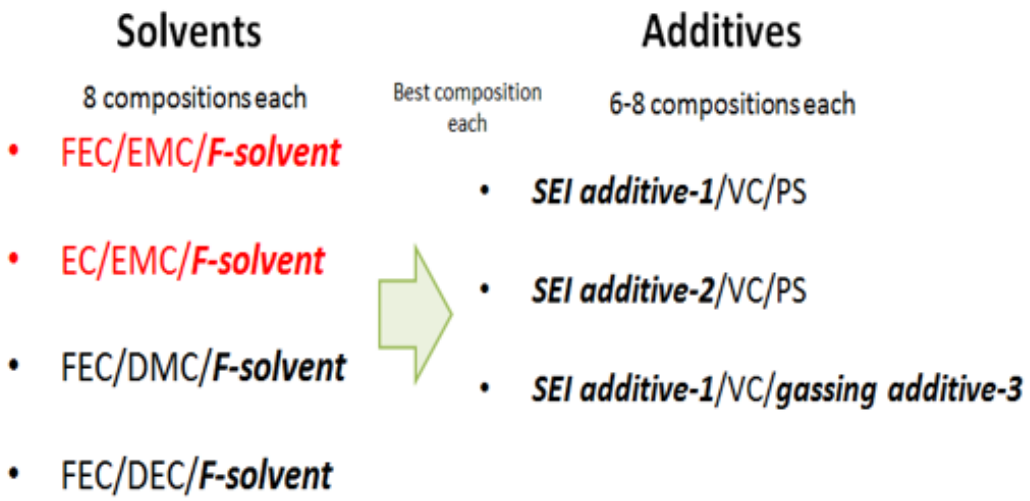

Table I. shows an explicit overview of the systems selected for study. Four solvent combinations all containing Daikin proprietary F-solvent (FE fluoroether) are being optimized with different carbonate solvents (DEC (diethyl carbonate), EMC (ethyl methyl carbonate), DMC (dimethyl carbonate) varied with (FEC (fluoroethylene carbonate/EC (ethylene carbonate) substitution. The gassing additives were PS (propane sultone) or a fluorinated sulfonate (FS). The SEI additives were VC (vinylene carbonates) and two types of cyclic fluorinated carbonate.

The tabulated electrolyte solvent/additive combinations were examined and optimized by use of PDCA (Plan-Do-Check-Act) cycles. A total of 4 PDCA cycles were completed which include 2 cycles for solvent, 1 cycle for SEI additive, and 1 cycle for gassing additive optimization. As a definition for this study, solvents are defined as components with >10% v/v and additives are materials with <5% w/w in the finished electrolyte.

The initial set of measurements was to determine voltage stability of the hydrocarbons and fluorocarbons to be used in the study. Figure 8. shows the linear scan voltammetry (LSV) of several of the candidate materials. The scans are completed using a platinum working electrode

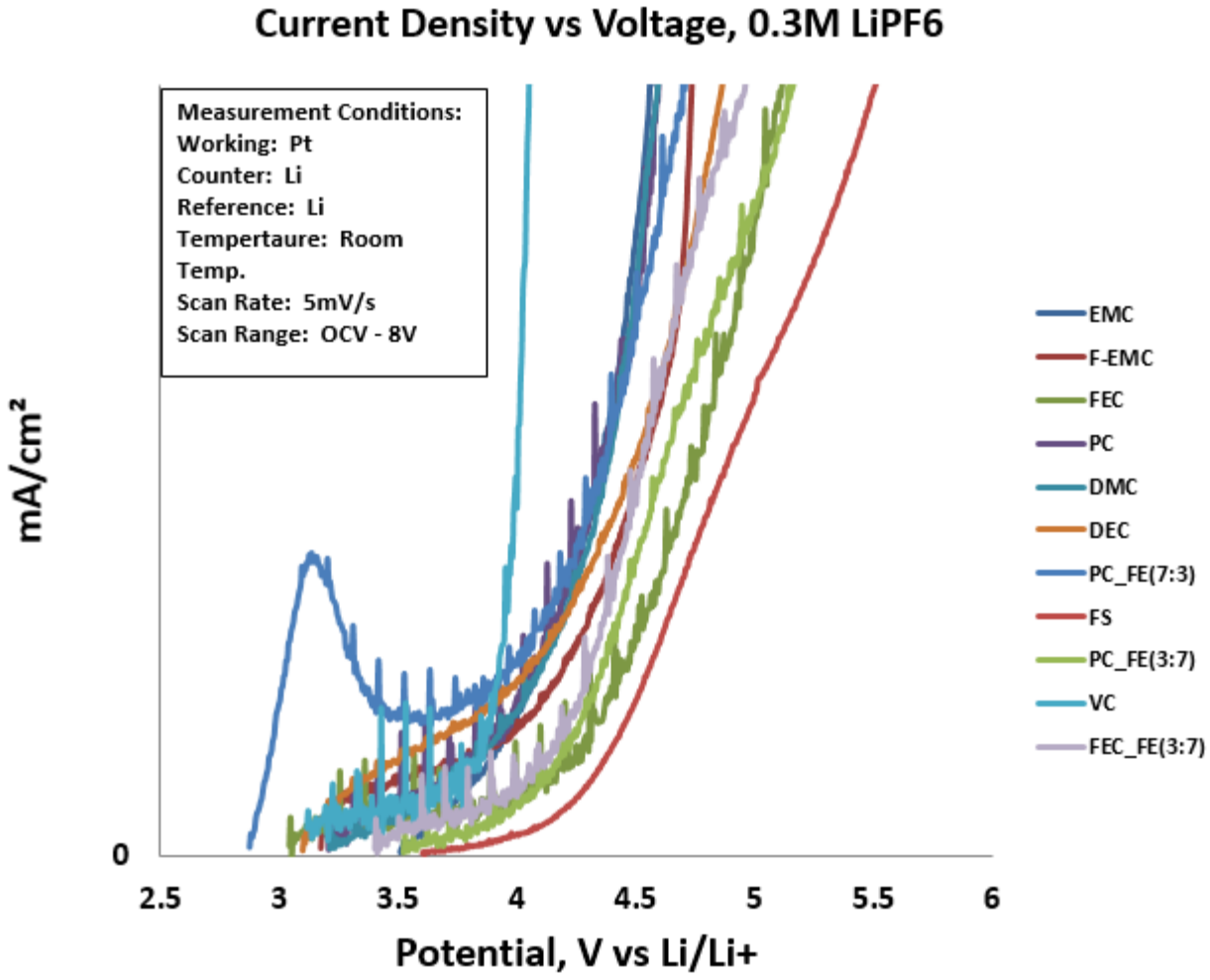

Figure 8 Linear Scanning Voltammetry Scans for all candidate solvent materials in the present study

against lithium metal counter and reference electrodes. The materials scanned are hydrocarbons

(PC (propylene carbonate), EMC (ethyl methyl carbonate), DEC (diethyl carbonate), DMC (dimethyl carbonate), VC (vinylene carbonate)), fluorocarbons FEC hyl carbonate) and mixtures thereof. In all cases, the fluorocarbon/fluorocarbon mixtures have a higher decomposition voltage. The noise in the signals is due to contact resistance of the alligator clips. In all cases, the fluorocarbon analog/substitutes for hydrocarbon components in existing conventional electrolyte show higher voltage stability.

The following LSV scan (Figure 9) shows a direct comparison of the conventional additive vinylene carbonate with a fluorocarbon additive mixture (FEC/fluoroether). Both of these materials are proposed as SEI forming additives. This data clearly shows that vinylene carbonate

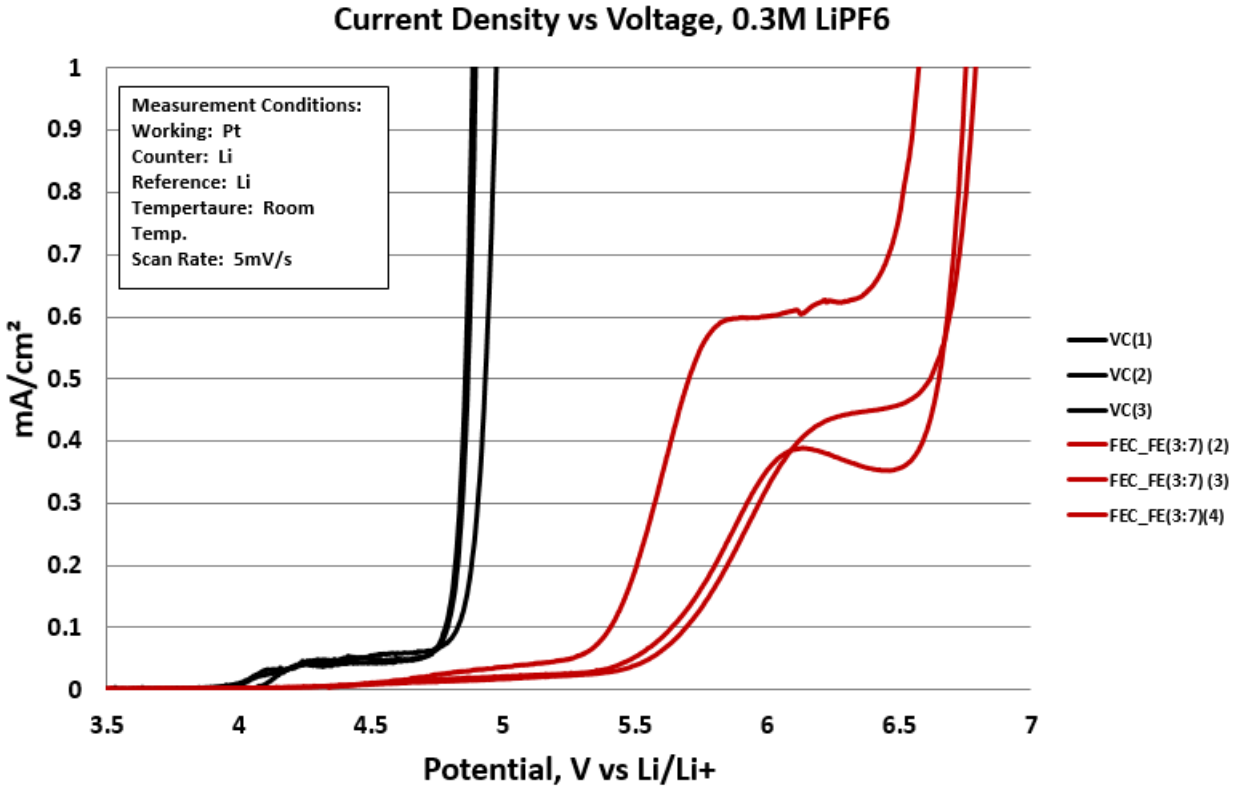

Figure 9. Linear Scanning Voltammetry for two different additive packages – vinylene carbonate (black) and fluoroaddtive mixture (red)

would not be an appropriate choice for high voltage (> 4.2 V).

Another major consideration in the selection of systems is the intrinsic conductivity of the electrolytes. As a general rule, fluorocarbon analogs of hydrocarbon electrolyte components have higher viscosity which leads to lower conductivity. This can be observed in viscosity and conductivity data where the hydrocarbon is replaced by a fluoroether in 10% v/v increments. The data in Figure 10. show 1.2 M $LiPF_6$ EC/EMC/fluoroether (20:80-x, x) where x is the

volume percentage of fluoroether added to the electrolyte. The electrolyte with x = 0 has a conductivity of 9.7 mS/cm and is not shown on the graph.

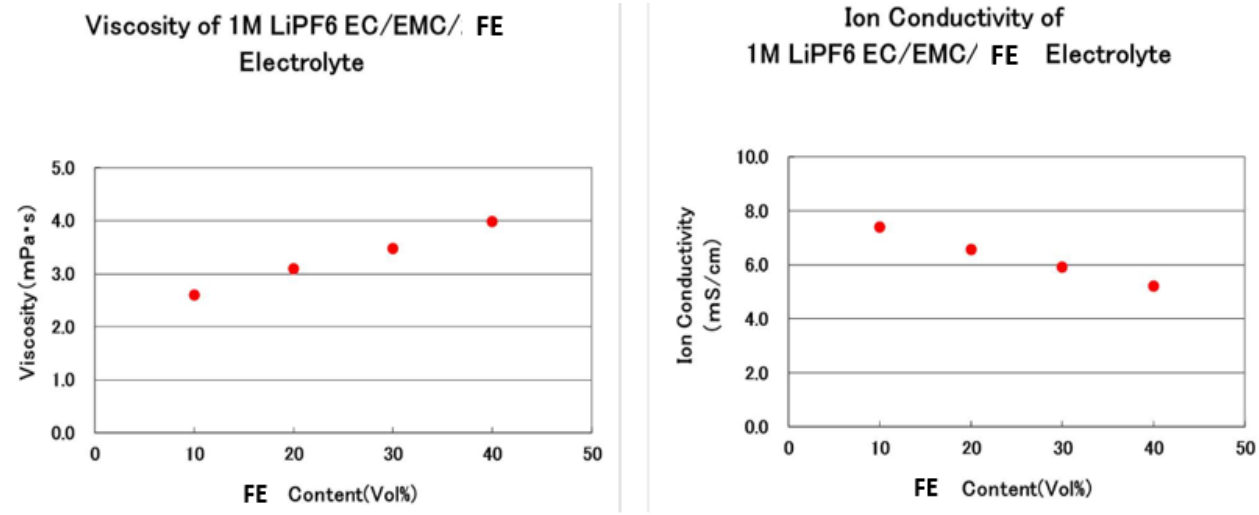

Figure 10 Conductivity as a function of temperature for various hydrocarbon/fluorocarbon mixtures to assess effect of fluoroether concentration (D7), salt concentration, FEC vs. EC, and hydrocarbon type

Conductivity of the chosen baseline electrolytes was measured and compared to variations of the same. The parameters that are being studied include hydrocarbon identity, fluoroether content, FEC vs. EC, and salt concentration. The aim of this exercise is to understand magnitude of conductivity change by affecting simple parameters. Some of the data is shown below.

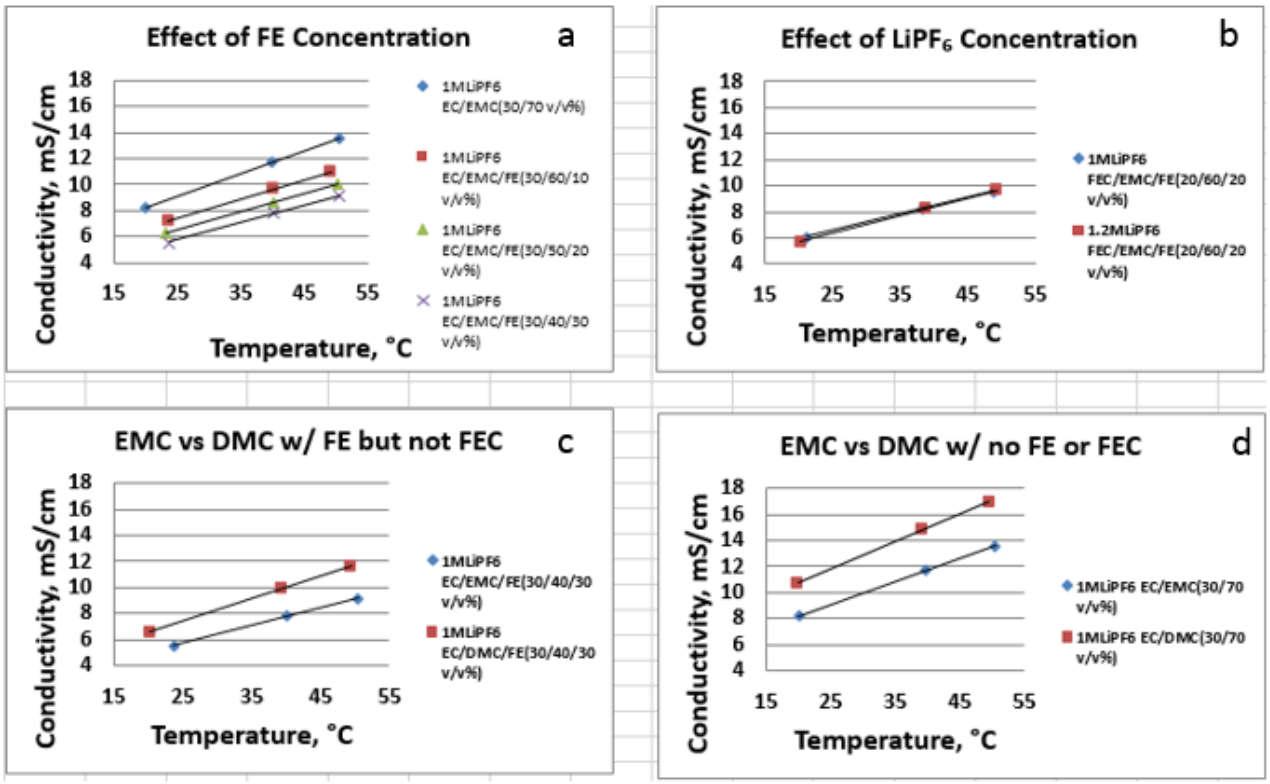

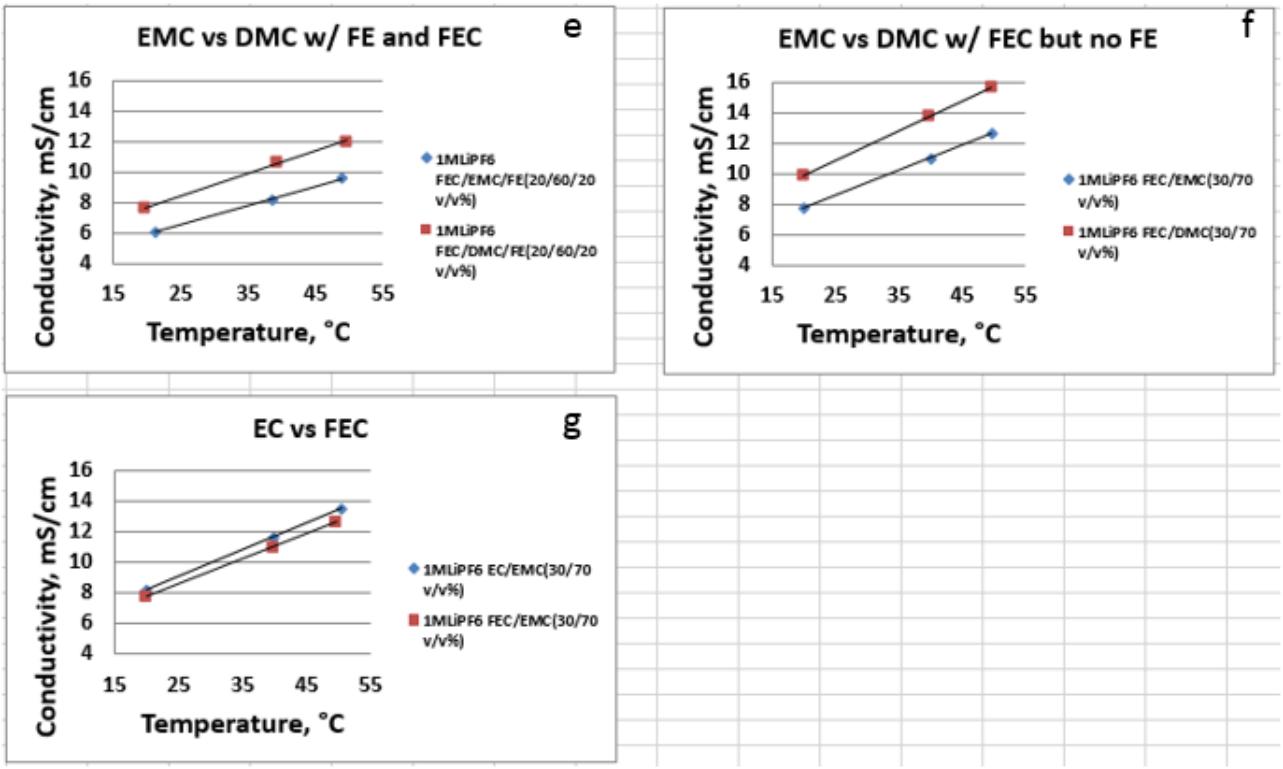

Figure 11 Conductivity as a function of temperature for various hydrocarbon/fluorocarbon mixtures to assess effect of fluoroether concentration (D7), salt concentration, FEC vs. EC, and hydrocarbon type

Conclusions from the conductivity data are as follows:

1) Decrease in conductivity is not linear with respect to fluoroether concentration (Fig11 a.)
2) In fluorinated baselines, there is no conductivity difference with salt concentration between 1 and 1.2 molar (Fig 11 b)
3) It is possible to affect the viscosity (and thus conductivity) by replacement of EMC with DMC. The conductivity magnitude change is proportionally same regardless of other electrolyte components. Conductivity of 1 M $LiPF_6$ FEC/DMC/fluoroether (2:6:2, 40% fluorocarbon) is same as 1M $LiPF_6$ EC/EMC (3:7, 0% fluorocarbon). Therefore, it is possible to optimize viscosity with prudent choice of solvent. (Fig 11 c, d, e, f)
4) Replacement of EC with FEC lowers conductivity (Fig 11 e, f, g)

As shown above, the choice of organic carbonate can have profound effect on the conductivity and rate performance. The lower viscosity solvents generally have a higher propensity for gassing due to higher vapor pressure (lower intermolecular interactions). Candidate electrolytes derived from both the voltage stability and conductivity testing were then examined in high temperature storage tests in charged NMC(111)/graphite batteries. The cells were filled with electrolyte, formed, and charged to 4.2 V. Cell volume measurements were made and the cells were then stored at 60 C for 72 hours. Post storage measurements included charge capacity, retention, recovery and cell volume and are shown in Fig 12.

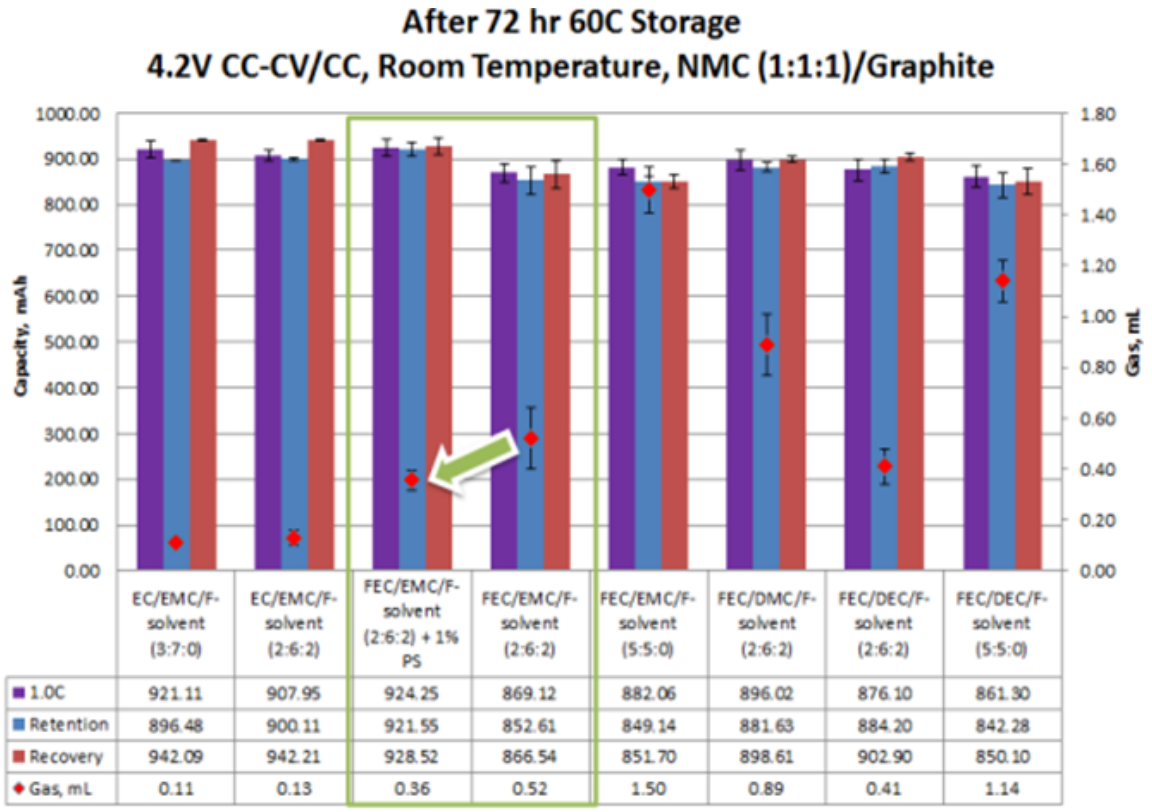

	EC/EMC/F-solvent (3:7:0)	EC/EMC/F-solvent (2:6:2)	FEC/EMC/F-solvent (2:6:2) + 1% PS	FEC/EMC/F-solvent (2:6:2)	FEC/EMC/F-solvent (5:5:0)	FEC/DMC/F-solvent (2:6:2)	FEC/DEC/F-solvent (2:6:2)	FEC/DEC/F-solvent (5:5:0)
1.0C	921.11	907.95	924.25	869.12	882.06	896.02	876.10	861.30
Retention	896.48	900.11	921.55	852.61	849.14	881.63	884.20	842.28
Recovery	942.09	942.21	928.52	866.54	851.70	898.61	902.90	850.10
Gas, mL	0.11	0.13	0.36	0.52	1.50	0.89	0.41	1.14

Figure 12 60 C storage data of several electrolyte compositions showing C-rate capacity, capacity retention, and capacity recovery (left axis). The gassing volume change is shown by red circles (right axis).

During the first two PDCA cycles property data of the solvent mixtures was collected and compiled. The properties under consideration are: conductivity, voltage stability, gassing, and battery properties (cell impedance, first capacity, OCV). Composition- property maps like the one shown in Figure13 for conductivity in an FEC/EMC/fluoroether mixture were constructed. In all cases, the most desired property (i.e. high conductivity, low gassing) is colored red and the least desirable is blue. The color scheme was then assigned numerical values normalized to 1 for best property and 0 for worst property. The intention is to overlay the maps to optimize base solvent compositions. An example of the methodology is shown in Figure 14 which shows addition of conductivity, voltage stability, gassing, and initial capacity maps. The data to construct these maps was generated from the experiments shown in Fig. 8 to 11. The best guess compositions from this technique will then be used as vehicles for different additive

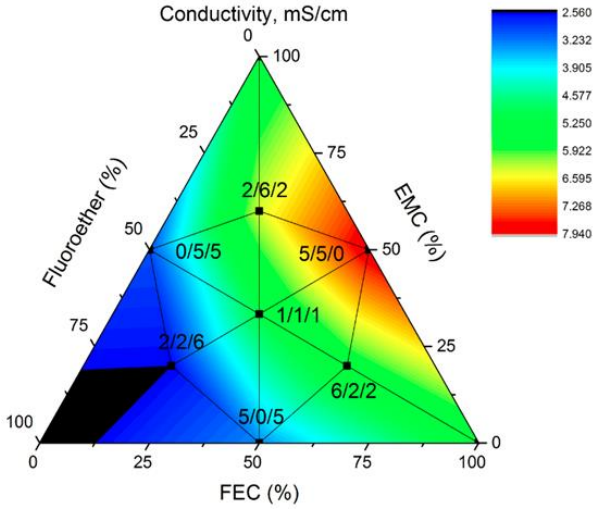

Figure 13 Composition-property map for conductivity of FEC/EMC/Fluoroether system. Red areas are optimal.

packages for enhanced cycle life. In practice, this also involves collecting real battery cycling data in parallel with the property mapping due to the fact that all the examined battery properties don't have equal weight when it comes to overall battery performance. An example of this is gassing in batteries having a much greater detrimental effect in comparison to first cycle capacity.

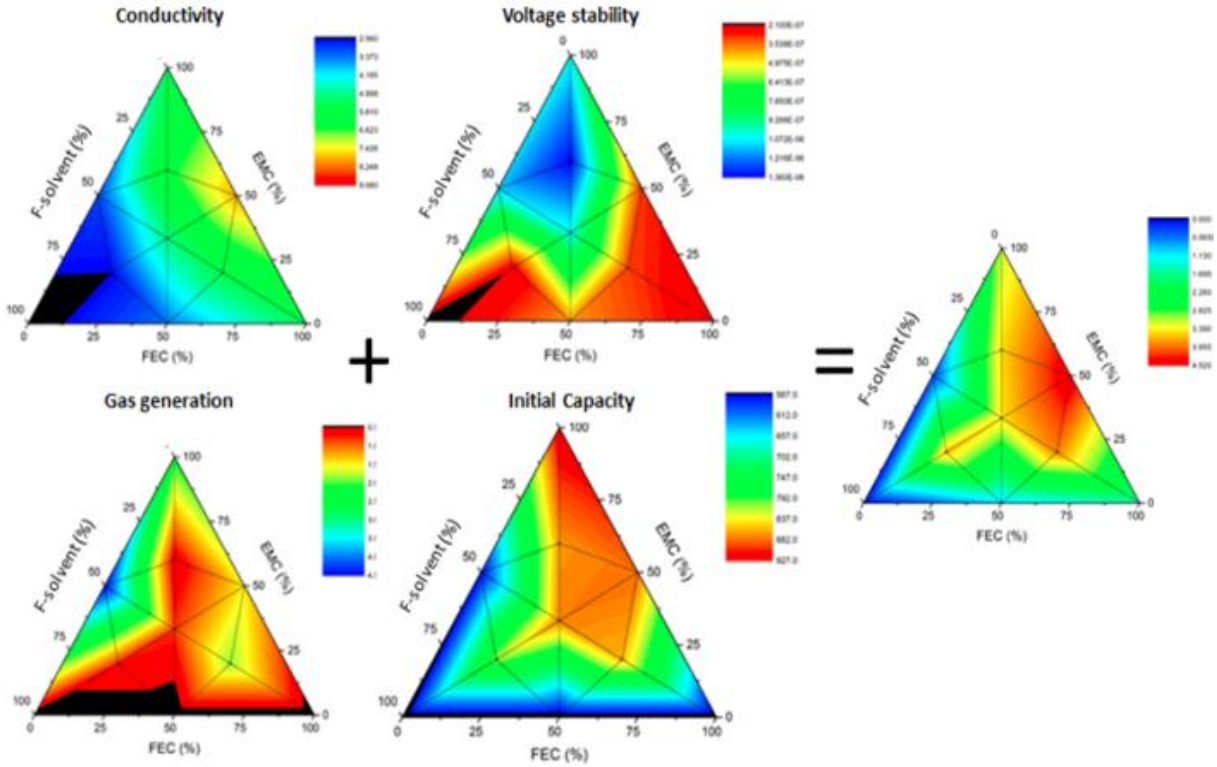

Figure 14 An example of addition of several composition-property maps which optimizes gas generation, initial capacity, conductivity and voltage stability.

At the completion of this exercise, the solvent package chosen consisted of 1.2 M $LiPF_6$ fluoroethylene carbonate (FEC) / ethyl methyl carbonate (EMC) / fluorosolvent (2:6:2).

Best guess electrolyte baseline properties

Two baseline compositions were chosen based on the property mapping analysis and existing cell data. They are: 1.0 M $LiPF_6$ EC/EMC (7:3) and 1.2 M $LiPF_6$ FEC/EMC/fluoroether (2:6:2) + additive which are nominally hydrocarbon and fluorocarbon electrolytes, respectively.

Figure 15. shows capacity vs rate for both of the baseline compositions as compared with two other compositions (1.2 M $LiPF_6$ FEC/DEC/fluoroether (2:6:2) + additive, 1.2 M $LiPF_6$ FEC/EMC/fluoroether (2:5:3) + additive). The fluorocarbon baseline (red trace) shows a 2-4% lower capacity than the hydrocarbon baseline (black trace) which is expected due to the increased viscosity/decreased conductivity of the fluorocarbon electrolyte. The slopes of the two curves are parallel out to 2 C. In contrast, the two additional electrolytes show marked decrease

in capacity between 1C and 2C. The cells were stored at 60 C for 72 hours and the experiment repeated. The performance trends are the same both before and after storage.

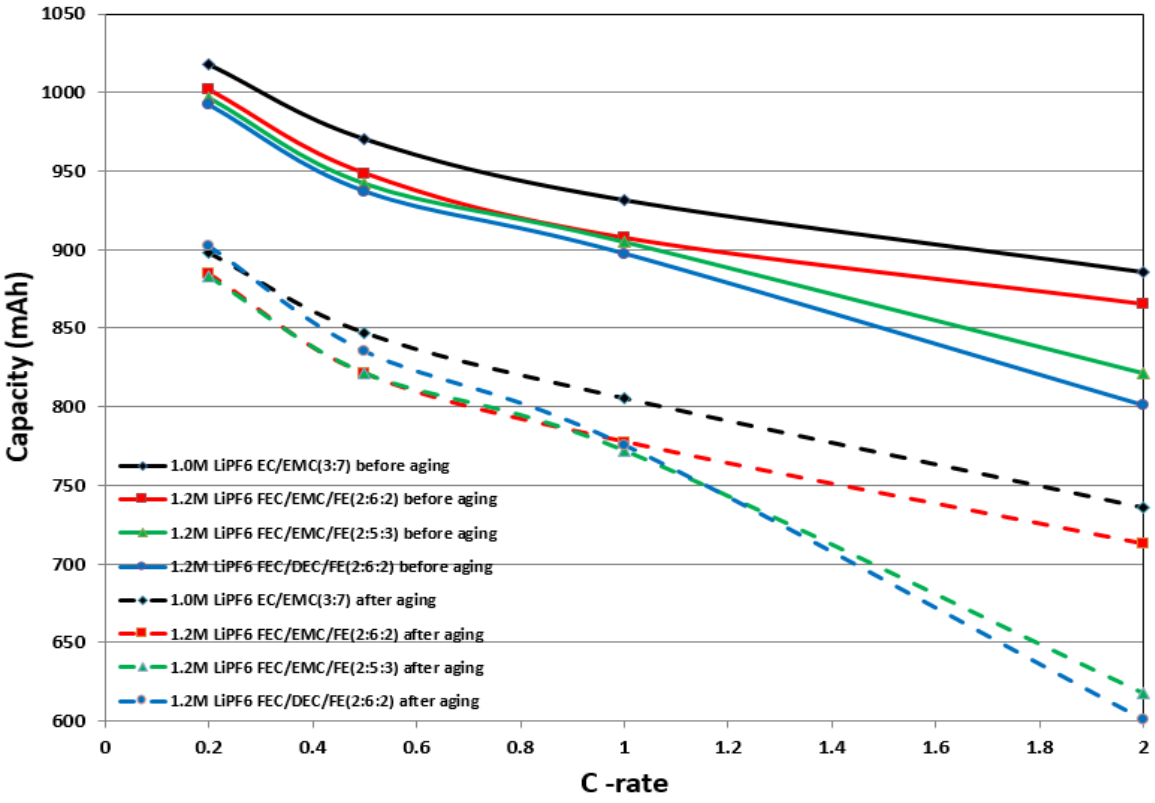

Figure 15 Capacity vs. C-rate for the baseline hydrocarbon electrolyte (1.0 M $LiPF_6$ EC/EMC (3:7) and fluorocarbon electrolyte 1.2 M $LiPF_6$ FEC/EMC/fluoroether (2:6:2)

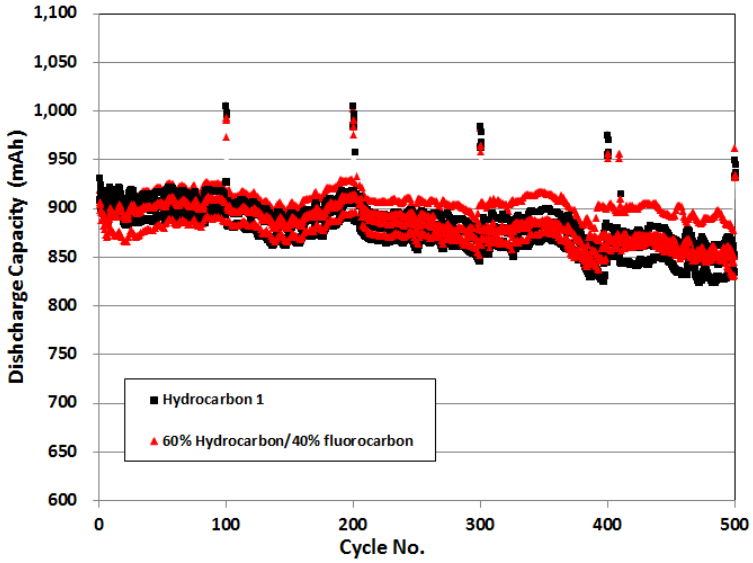

Figure 16 C-rate room temperature cycling for the baseline hydrocarbon electrolyte (1.0 M $LiPF_6$ EC/EMC (3:7) and fluorocarbon electrolyte 1.2 M $LiPF_6$ FEC/EMC/fluoroether (2:6:2)

Figure 16. shows the room temperature C-rate cycle testing of the baselines as measured in NMC/graphite commercial cells. A capacity check at 0.2 C is completed every 100 cycles. There is no appreciable difference in the cycle performance at 1C even in an electrolyte which contains nominally 40% fluorocarbon solvent. The noise in the experiment is due to temperature variations in the room.

Due to the post 60 C storage results in Figure 17., a temperature stability

investigation was completed on the two baseline compositions to determine that no thermal decomposition occurs during storage. The baseline electrolytes (EMC/EC 7:3) and (FEC/EMC/FE 2:6:2) were compared to a third electrolyte which contained fluoroether FE but with EC instead of FEC to delineate thermal stabilities of hydrocarbon, FEC, and the fluoroether. The three compositions were prepared then stored neat at RT, 60 C and 85 C. The composition containing FEC had a noticeable color change at 85 C (see graph below). The color change is due to decomposition of the $LiPF_6$ salt and has been previously studied.[31] NMC/graphite cells were then filled with these electrolytes and the performance was measured. The results in Figure

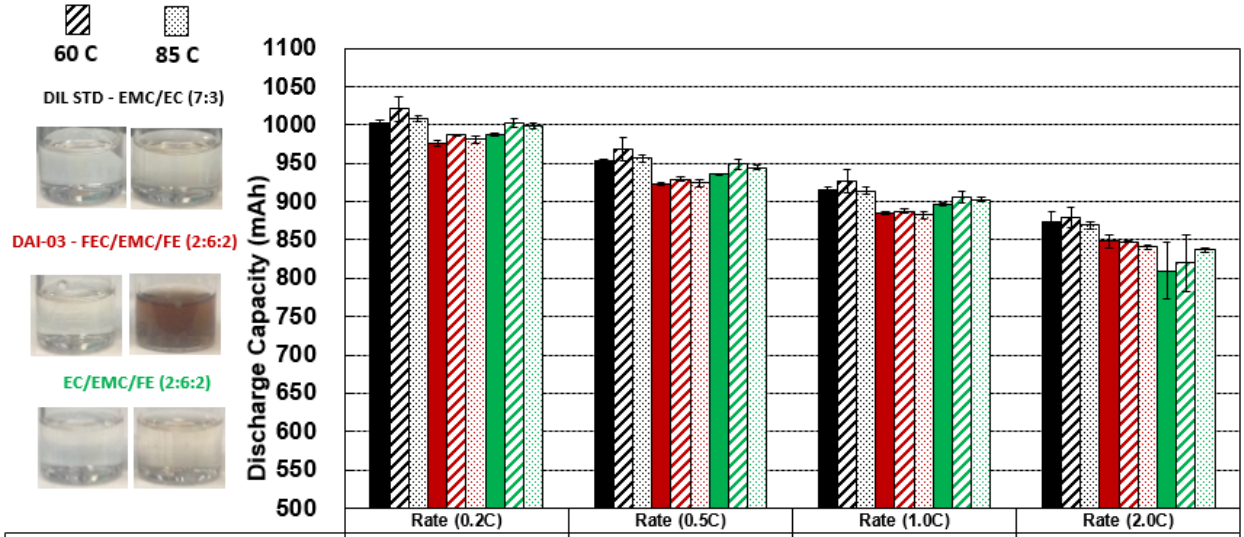

	Rate (0.2C)	Rate (0.5C)	Rate (1.0C)	Rate (2.0C)
Charged (DIL STD)	1003	954	916	874
60°C Electrolyte Storage (DIL STD)	1021	969	926	880
85°C Electrolyte Storage (DIL STD)	1009	956	914	869
Charged (DAI-03)	977	923	885	849
60°C Electrolyte Storage (DAI-03)	987	929	888	848
85°C Electrolyte Storage (DAI-03)	981	924	882	841
Charged (EC/EMC/FE)	988	935	897	810
60°C Electrolyte Storage (EC/EMC/FE)	1003	949	906	820
85°C Electrolyte Storage (EC/EMC/FE)	998	945	903	837

Figure 17 Capacity vs rate date for the baselines the baseline hydrocarbon electrolyte (1.0 M $LiPF_6$ EC/EMC (3:7) and fluorocarbon electrolyte 1.2 M $LiPF_6$ FEC/EMC/fluoroether (2:6:2). There are 3 conditions: fresh electrolyte, electrolyte preheated to 60 C and

17 showed no difference in rate or capacity when discharged from 4.2 V even with apparent decomposition of the FEC electrolyte.

However, after the fully charged cells are stored at 85 C for 72 hours, there is pronounced gassing in cells containing FEC electrolyte regardless of the electrolyte aging protocol. This is represented by the red diamonds in Figure 18. This enhanced gassing leads to diminished cell performance in capacity retention, recovery and rate capability. The most pronounced effect of gas generation is in long term cycling. It is suggested that all oven aging protocols do not exceed 60 C to get true performance characteristics of FEC containing electrolytes.

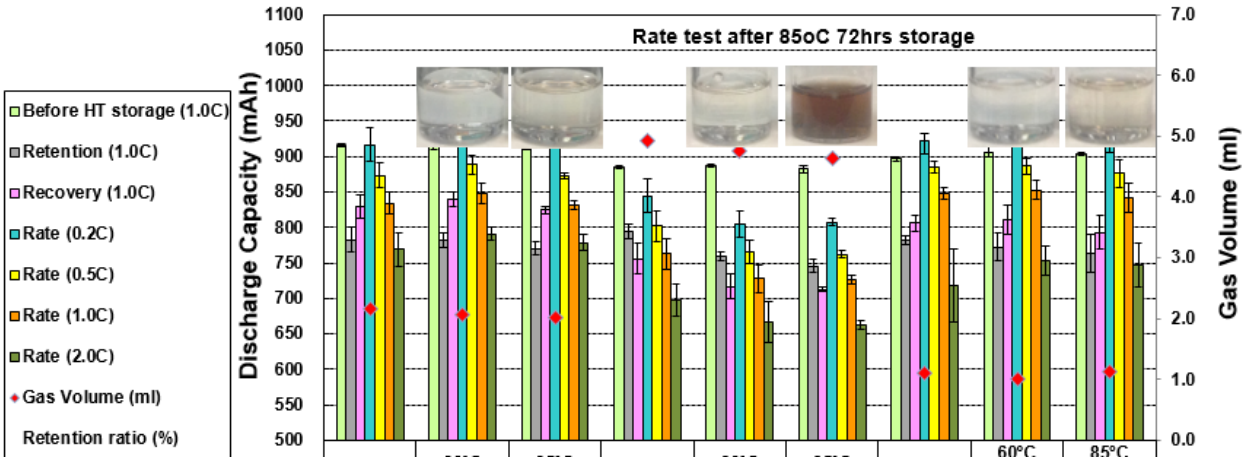

	Charged (DIL STD)	60°C Electrolyte Storage (DIL STD)	85°C Electrolyte Storage (DIL STD)	Charged (DAI-03)	60°C Electrolyte Storage (DAI-03)	85°C Electrolyte Storage (DAI-03)	Charged (EC/EMC/FE)	60°C Electrolyte Storage (EC/EMC/FE)	85°C Electrolyte Storage (EC/EMC/FE)
Before HT storage (1.0C)	916	926	914	885	888	882	897	906	903
Retention (1.0C)	782	782	770	794	760	745	782	772	764
Recovery (1.0C)	830	840	825	756	717	713	806	810	793
Rate (0.2C)	916	941	923	844	805	808	923	926	915
Rate (0.5C)	874	889	872	802	765	762	885	886	876
Rate (1.0C)	834	847	831	763	728	726	849	853	841
Rate (2.0C)	769	791	778	698	667	663	718	753	746
Gas Volume (ml)	2.15	2.07	2.01	4.94	4.77	4.65	1.11	1.00	1.12
Retention ratio (%)	85	84	84	90	86	84	87	85	85

Figure 18 Rate data for the electrolyte (fresh, preheated 60 C and preheated 85C) on the left axis. Gassing volume change is denoted by red diamonds (right axis)

Cell performance impact at higher voltages

Using the commercial NMC/graphite commercial cells, the cells were cycled to 4.2, 4.3, 4.35, 4.4, 4.5, 4.6 and 4.8 V to determine the energy gain attained by cycling at higher voltage. The energies are calculated by integrating the capacity curves with respect to voltage. The energies are normalized to the energy at 4.2 V. Figure 19 shows the capacities and normalized energies for commercial NMC/graphite cells discharged at both low (0.2 C, top panels) and moderate/high rate (1C, bottom panels) for the baseline electrolytes containing hydrocarbon (right panels) and fluorocarbon/hydrocarbon (left panels). It can be seen that charge/discharge at 4.5 V results in a 25% and 31% energy gain for cells containing hydrocarbon and fluorocarbon/hydrocarbon electrolytes, respectively. The results shown in the graph are only the first charge/discharge cycle. It has been noted that there appears to be a decomposition of hydrocarbon electrolyte at or above 4.35 V which is also consistent with the discontinuity observed in the energy as a function of discharge voltage. There is also a discontinuity in the curves between 4.5 and 4.6 V for the fluorocarbon. It is not known whether this discontinuity can be attributed solely to the electrolyte or whether it is cell dependent (i.e. cathode crystal structure change). While data is shown for 4.8 V, the data can only be realized for one cycle due to the destabilization of the cathode structure when too much lithium is removed.

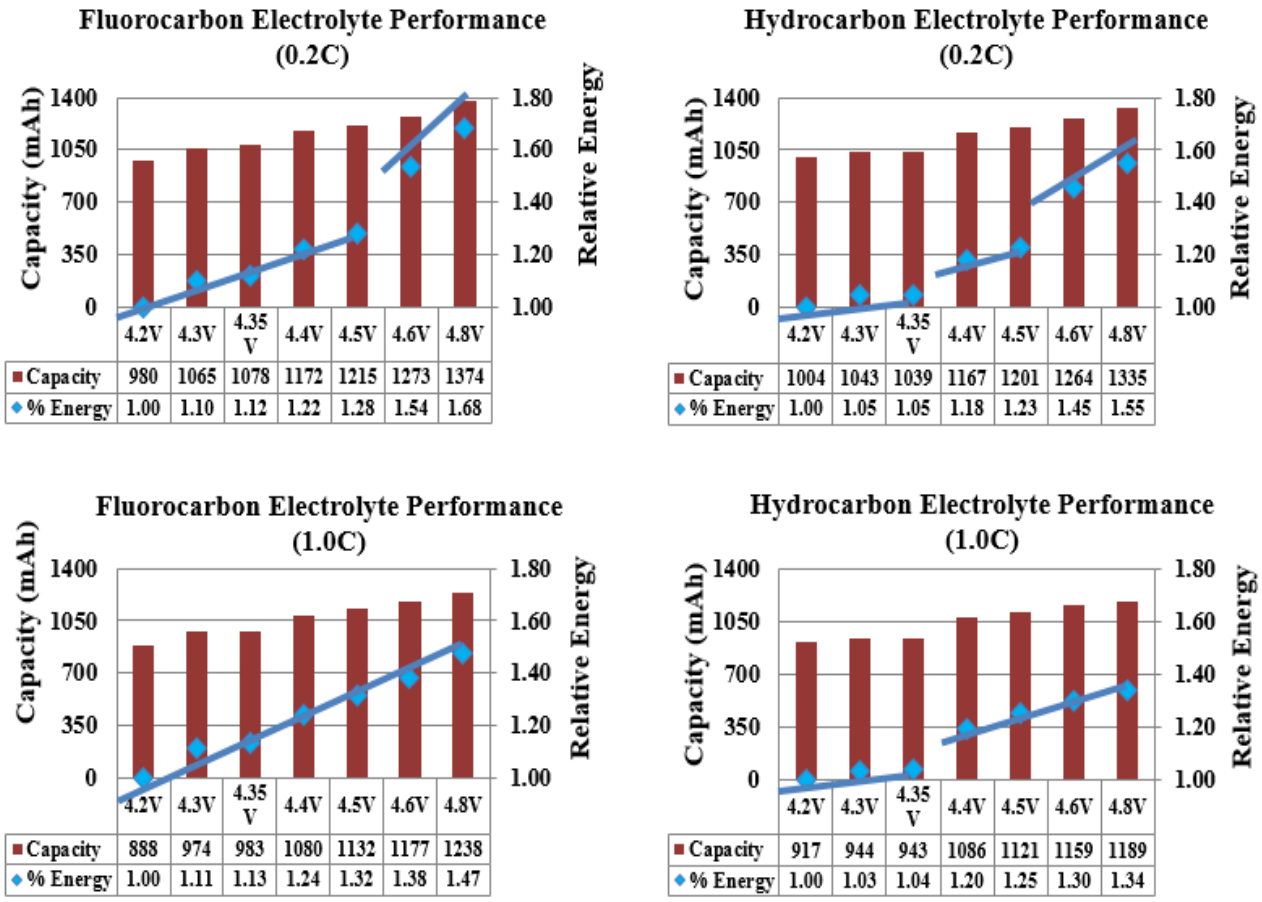

Figure 19 Capacity vs voltage for fluorocarbon (left panels) and hydrocarbon (right panel) filled NMC111/graphite cells. This is shown for both low rate (0.2 C, top panels) and moderate rate (1 C, bottom panels). The blue diamonds show the cell energies normalized to the energy at 4.2 V

Earlier experiments indicated that the threshold voltage for hydrocarbon decomposition in electrolyte was around 4.35 V. NMC111/graphite cells were filled with the optimized electrolyte solvent package (1.2 M $LiPF_6$ FEC/EMC/F-solvent + 1% propane sultone PS). The PS was added as an additional precaution against gassing. In addition, cells were also filled with a hydrocarbon control 1.0 M $LiPF_6$ EC/EMC (3:7) + 1% PS. The cells were then cycled at 1 C and 60 C. The upper cycling voltages were selected to be below (4.2 V), at (4.35 V) and above (4.5 V) the hypothesized decomposition threshold voltage.

The data is shown in Figure 20 with the hydrocarbon control and Daikin fluorinated electrolytes in the top and bottom panels respectively. The hydrocarbon control cells cycled at 4.5 V die very quickly and cells cycled near the 4.35 V decomposition voltage also eventually die. The cells filled with Daikin fluorinated electrolyte continue to cycle at 250 cycles and 60 C at all three voltages.

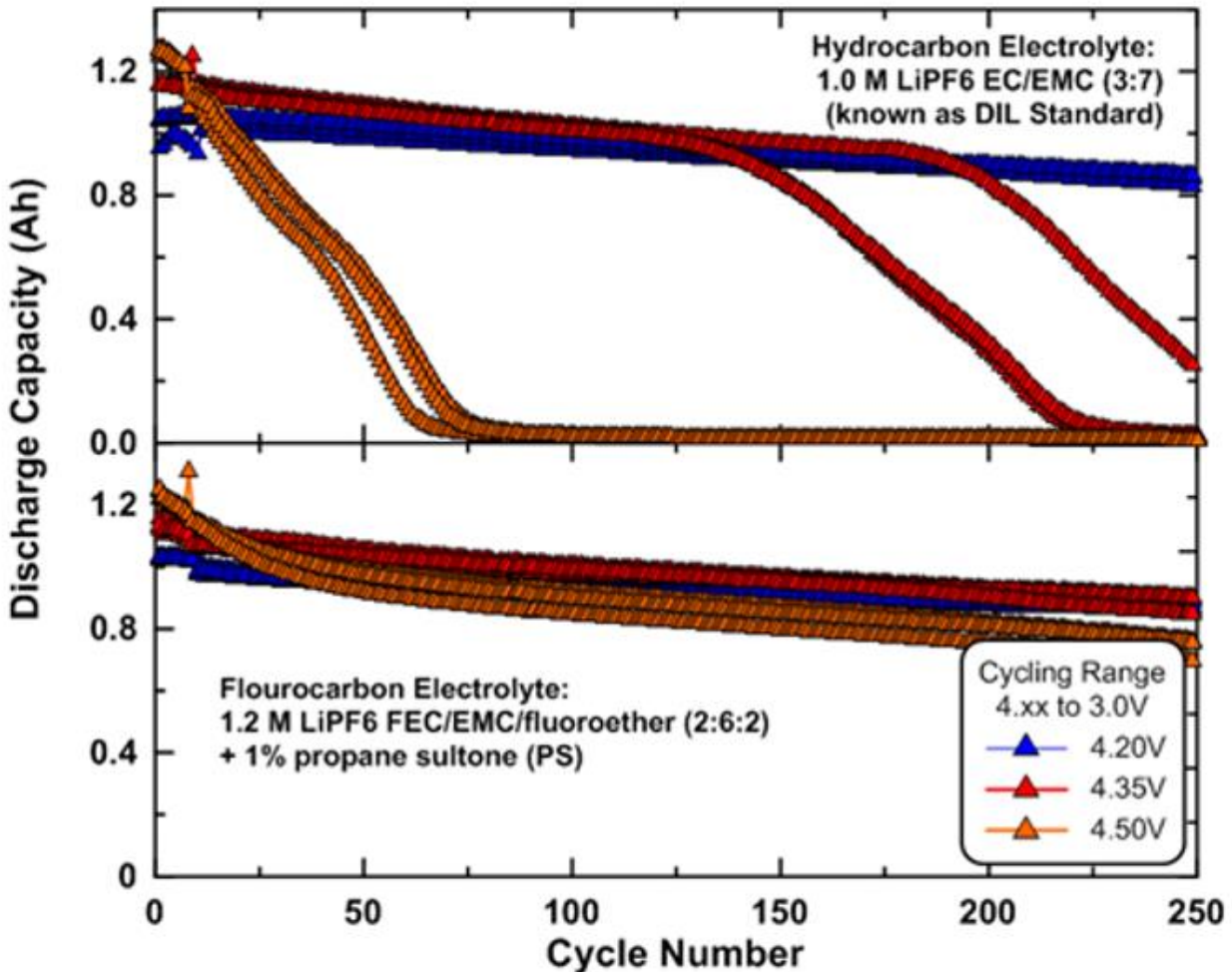

Figure 20 Accelerated (60 C, 1 C) cycle life data for hydrocarbon electrolyte (top panel) and fluorocarbon electrolyte (bottom panel) at three voltages (4.2, 4.35 and 4.5 V)

Figure 21. shows both the hydrocarbon and fluorocarbon cells after the cycling experiment from Fig. 19 The photos show visible gassing in the hydrocarbon cells which is not observed in the fluorocarbon cells. The data on the right side shows the gas volume generated at 4.2, 4.35 and 4.5 V post cycling.

As a comparison of these electrolytes across cell chemistries, Figure 22 shows the energy vs. voltage analysis for a different chemistry ($LiCoO_2$ (LCO)/Si-graphite composite) as an example. In this experiment, the LCO/Si-graphite composite cells were a commercial cell balanced for 4.4 V operation. Figure 22. shows the normalized energy vs voltage analysis of these cells similar to the analysis shown in

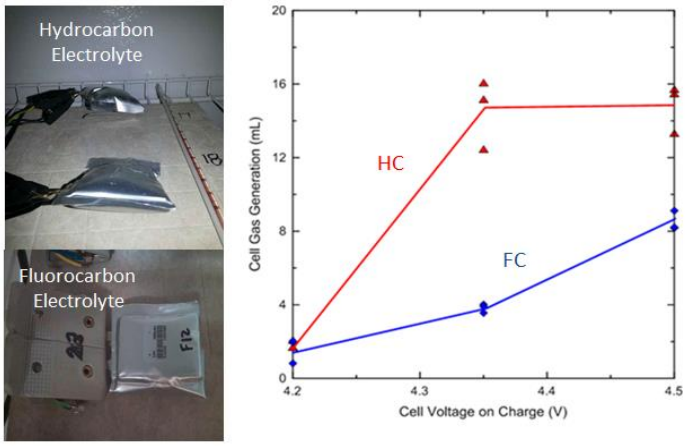

Figure 21 Photographs and gas volume change data post cycling test (previous figure)

Figure 19. Again, there is a substantial energy gain (app. 28 %) when discharging the cell at 4.5 V. The energy vs. voltage performance for this chemistry shows a discontinuity between 4.5 and 4.6 V. The data at 4.8 V is only added for completeness but clearly shows the LCO structure cannot survive high level of de-lithiation.

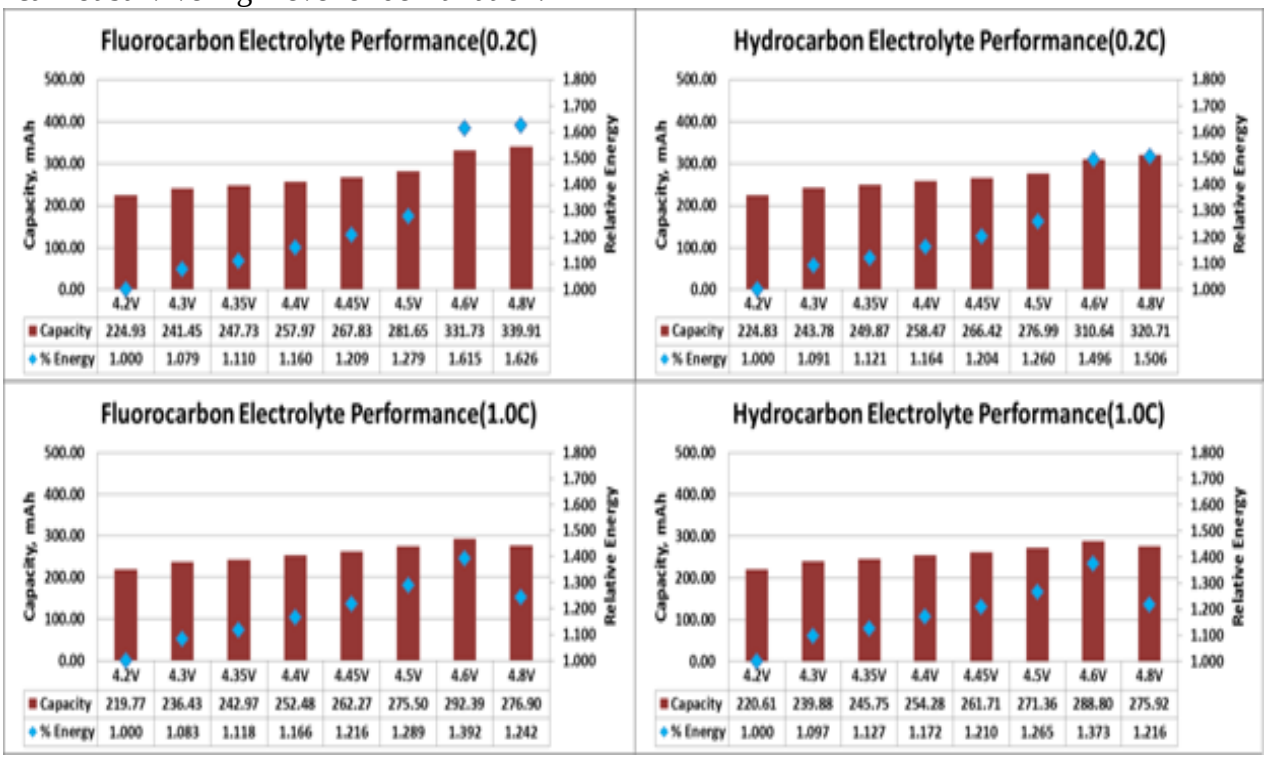

Figure 22 Capacity vs voltage for fluorocarbon (left panels) and hydrocarbon (right panel) filled LCO/graphite cells. This is shown for both low rate (0.2 C, top panels) and moderate rate (1 C, bottom panels). The blue diamonds show the cell energies normalized.

Cycle life testing was initiated to determine whether cell failures and swelling behavior at higher voltages occurred independent of cell chemistry. Figure 23 shows the cycle life of hydrocarbon and fluorocarbon electrolytes in LCO/ Si Composite cells cycled at 4.2, 4.4, and 4.6 V which are lower than, near and above the hypothesized hydrocarbon decomposition voltage, respectively. At 4.2V, cycle life in both hydrocarbon (black) and fluorocarbon (red) is stable, with the fluorocarbon electrolyte maintaining better capacity retention out to 1000 cycles. At 4.4V, the hydrocarbon electrolyte

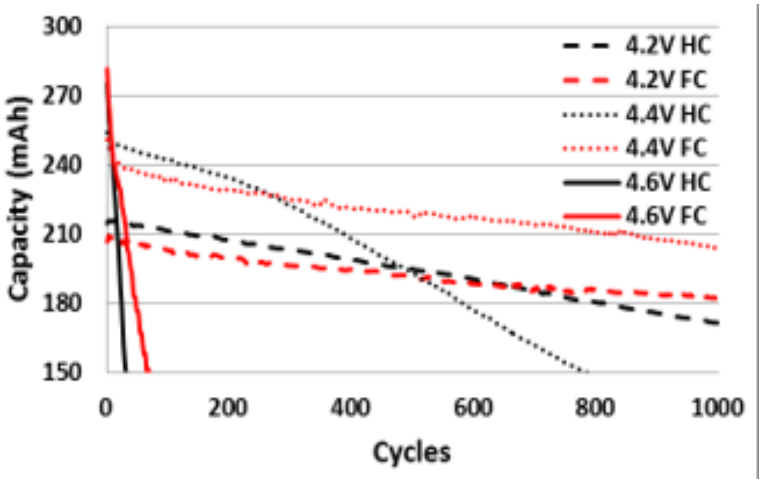

Figure 23 Room temperature cycle life data for LCO/Si composite cells at three different voltages (4.2, 4.4, 4.6 V)

began to fail, with 80% capacity retention reached at approximately 425 cycles. The fluorocarbon electrolyte maintained capacity retention above 80% out to 1000 cycles, where the testing was concluded. As was seen with the previous cell chemistry, at 4.6V, both electrolyte

Figure 24 Photographs of LCO/SI composite cells post cycle life test (from previous figure)

formulations failed rapidly, although the fluorinated electrolyte showed better performance than the hydrocarbon electrolyte. Figure 24. shows photographs of cells containing both fluorinated (bottom row) and hydrocarbon electrolyte (top row) fresh and after being cycled to 4.2, 4.4 and 4.6 V. There is significantly less gassing than in the NMC111/graphite cells shown above. The differences in the two experiments are probably due to the nickel content in the cathode. There is also not significant difference between the fluorocarbon and hydrocarbon containing cells.

Non gas cell swelling (Table II) was measured after cycling was completed. At 4.2V, the cells with hydrocarbon electrolyte exhibited a 14% increase in cell thickness, whereas the fluorocarbon cells showed no signs of swelling. This trend continued at 4.4V, with the hydrocarbon cells having a 28% increase in thickness, while the fluorocarbon cells showed no thickness increases. Both hydrocarbon and fluorocarbon cells cycled at 4.6 V exhibited non gas cell swelling of 18-20%. The trend in increasing cell thickness are consistent with the decrease in cycle life of the cells.

Table II. Cell gauge thickness for both hydrocarbon and fluorocarbon electrolyte as a function of voltage

Average Cell Thickness		
	Hydrocarbon	Fluorocarbon
Fresh Cell	0.177"	
4.2V	0.202"	0.168"
4.4V	0.228"	0.176"
4.6V	0.213"	0.209"

Optimization of additives

Following the choice of the appropriate solvent mixture (components, volume ratio) and selection of voltage appropriate additives, experiments were then completed to optimize an additive mixture for the NMC111/graphite cell chemistry for operation above 4.35 V. It should be noted that additives by definition are those components existing in a <5% by weight concentration in the mixture. The solvents are considered to be anything in >10% concentration by volume. The additives developed at Daikin may have several functionalities such as:

1. Surface modification agents for anode and/or cathode
2. Direct interaction with contaminants such as HF and

3. Agents which affect solubility of metal ions at high voltage.

The additive and solvent mixtures described in this report were optimized for NMC111/graphite. It will be necessary to develop custom formulations dependent on cell chemistry and operational parameters (voltage, temperature, rate).

Preliminary work for PDCA cycle 3 (additive optimization) involved understanding the comparison between known film forming additives and those proposed by Daikin. It is believed that FEC works well for two reasons: it improves the voltage stability of the solvent mixture and it works like an SEI layer making additive. The comparison of FEC to Daikin cyclic fluorocarbonates (FA1, FA2) as well as hydrocarbon (VC, EC) SEI forming additives has been

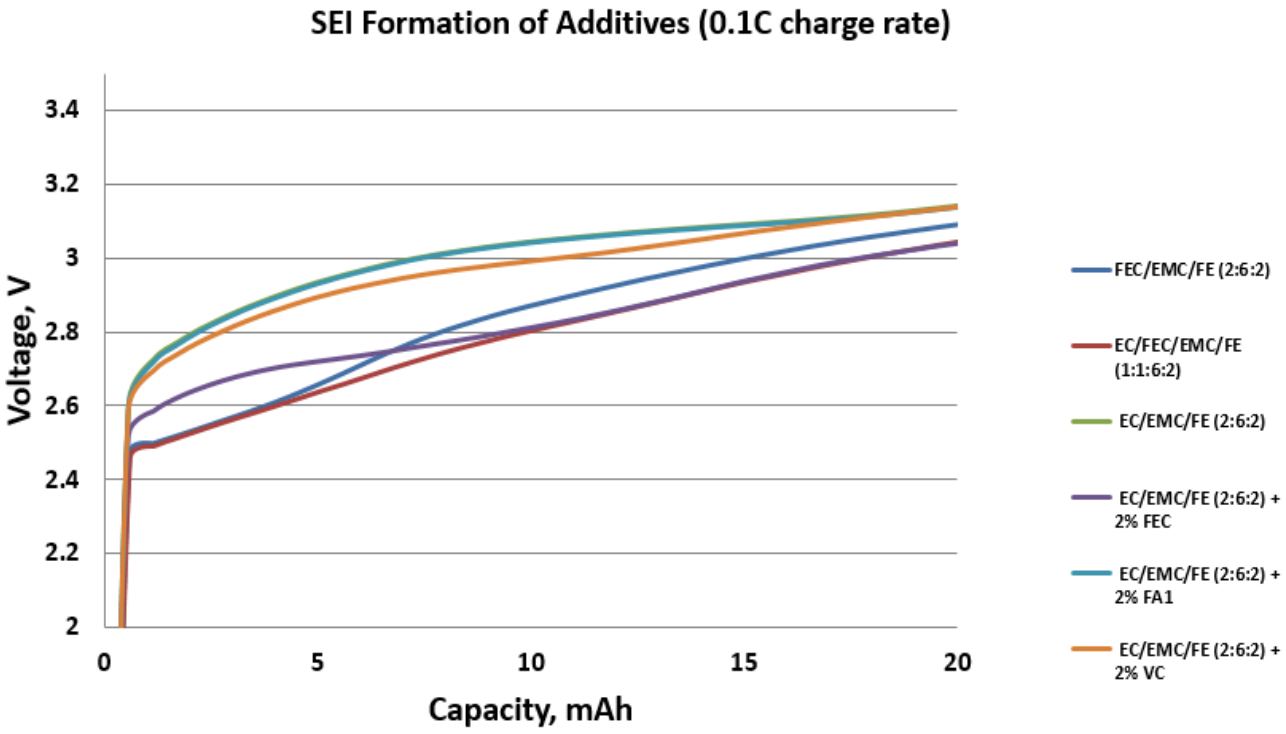

Figure 25 First charge curves for several electrolytes showing the film formation energy

examined. Examination of first charge cycle data is being used as the screening tool. The first charge data is measured for an electrolyte with and without the additive. The difference in energy between the two samples is considered to be proportional to the film formation energy. Figure 25 shows a comparison of FEC/FA1/VC. The data show that FEC has a bigger parasitic energy (film formation). It unclear that all the parasitic energy is due to surface film formation which would be proportional to the concentration of additive as well as surface area of carbon. Measurements were made to vary the FEC concentration (from 2 – 20 %) and watch the parasitic energy to determine an upper limit for forming the film (i.e. if the parasitic energy keeps increasing with increasing FEC content than there is another process). The first charge as a function of FEC content is shown in Figure 26. The parasitic energy grows with the FEC concentration and the upper limit of the parasitic energy as a function of FEC concentration is

still not known. This possibly suggests another decomposition phenomenon is occurring which is not surface area restricted.

An additional round of first charge experiments were done on the several electrolyte mixtures at various temperatures. The hypothesis was that due to wetting characteristics and mobility of fluorochemicals that we would be able to see more efficient film formation if the batteries were formed at higher temperature. Some examples are shown below:

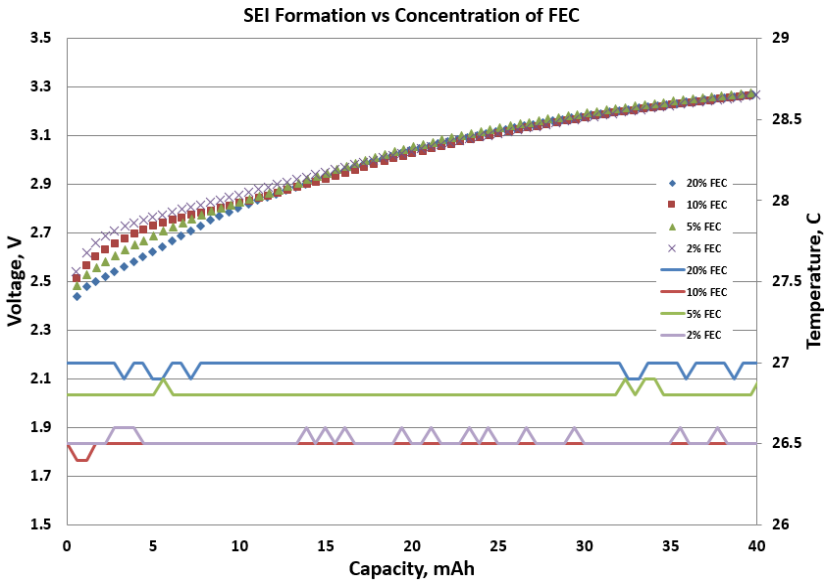

Figure 26 First charge curves show SEI formation as a function of FEC concentration

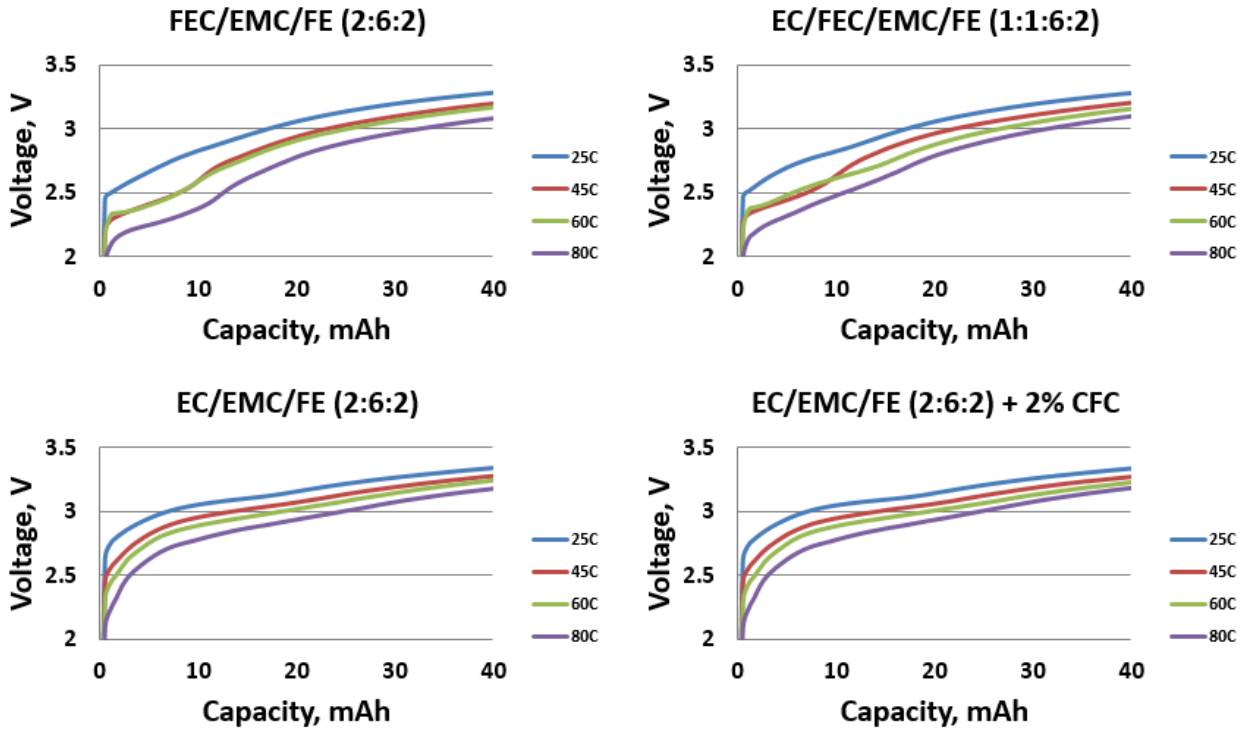

Figure 27 First charge curves for several electrolytes showing effect of FEC, EC, fluoroether (FE) and cyclic fluorocarbonate (CFC/FA1)

In general, the parasitic energy increased with higher temperature which would indicate more efficient film formation. However, when we cycled the batteries formed at 80 □C, the cycle behavior became poorer for the batteries containing FEC (see below data). This is attributed to the poor thermal stability of the FEC shown above.

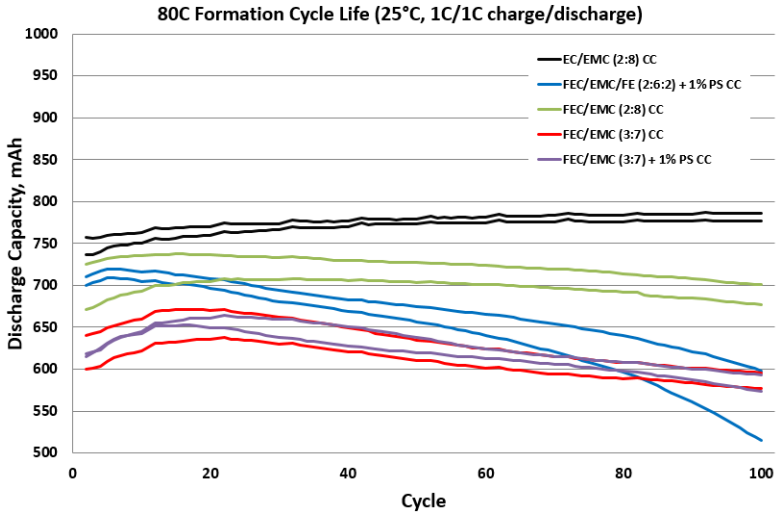

Figure 28 Cycle life of NMC111/graphite cells filled with several hydrocarbon and fluorocarbon electrolytes after being formed at 80 C

When the solvent mixture (1.2 M $LiPF_6$ FEC/EMC/F-solvent) was fixed, various combinations of additives were added. The finished electrolytes were then filled into the NMC111/graphite cells and were examined by high performance coulometric techniques as a screening tool. This work was completed at Coulometrics LLC and is based on the work of Jeff Dahn.[26-30] When several combinations were identified, new cells were constructed with the candidate electrolytes and were cycled to 4.5 V at 60 C. Figure 29 shows the cycling data for various combinations. The hydrocarbon control electrolyte (1.0 M EC/EMC 7:3) is included for reference. All other samples shown in this Figure 29 use the optimized Daikin solvent composition as a base. All of the electrolytes with the Daikin fluorinated solvent show same magnitude performance. The effect of the additives is to manipulate the slope of the cycle life curve. This experiment shows the best combination of additives to be 1% Z1 (gassing additive) + 1% FA1 (fluoro SEI formation additive)

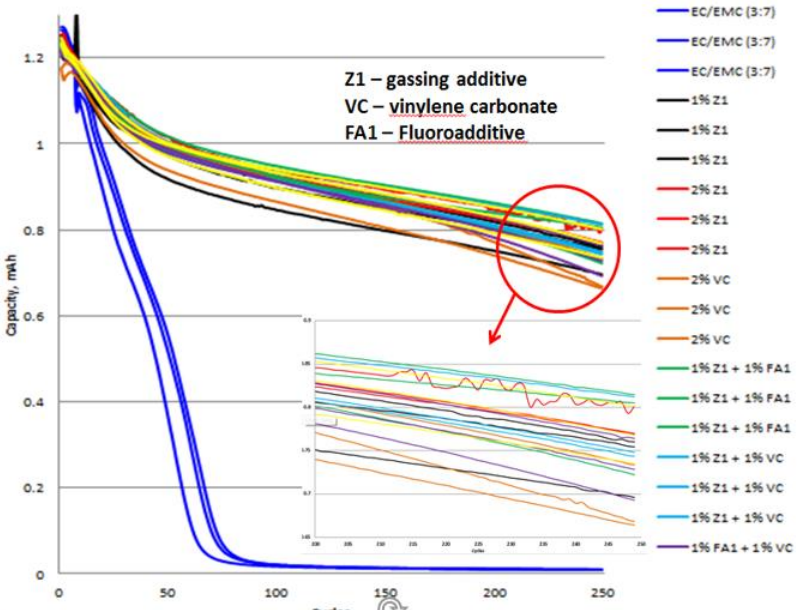

Figure 29 Cycle life (1C, 60 C, 3.0-4.5 V) of fluorinated electrolytes containing different additive packages. The hydrocarbon control electrolyte is shown in blue

Gassing measurements were also performed on various additive mixtures. The cells were filled with the same solvent mixture with variable additive mixtures. The cells were charged to 4.5 V and stored 72 hours at 60 C. The gas volume data

for these mixtures is shown in Figure 30. The primary result is that mixtures containing vinylene carbonate exhibit more gassing when operated at higher voltages.

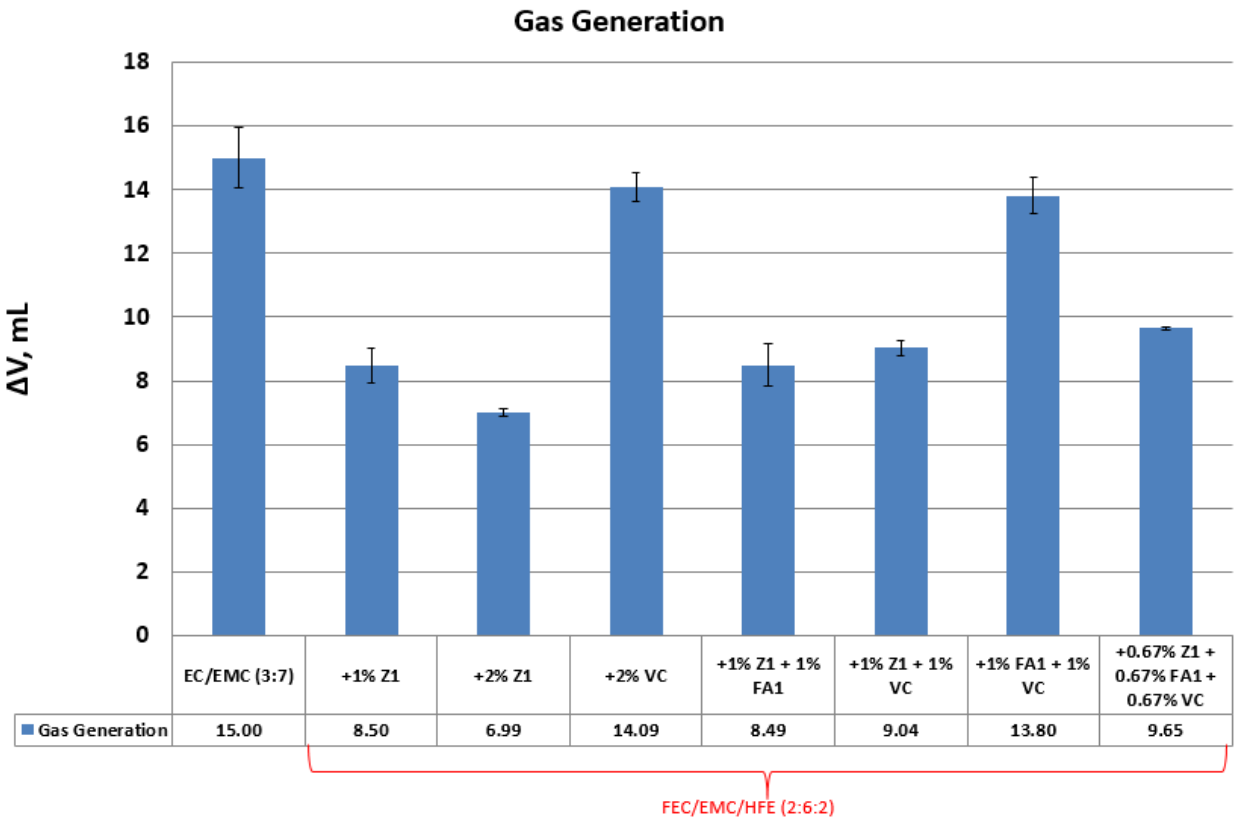

Figure 30 Gas volume for NMC111/graphite cells with various additive combinations after 60 C storage at 4.5 V.

External evaluation of preliminary cells

A set of preliminary cells were sent for external evaluation at Argonne National Laboratory. Complete details of the measurements can be found in Argonne's quarterly report. 10 1 Ah NMC111/graphite cells filled with best guess optimal electrolyte 1.2 $LiPF_6$ FEC/EMC/F-solvent (2:6:2) + 1% additive A were sent. The preliminary cells were sent before complete optimization of the additive package. The nominal tested capacity at 4.6 V was measured at 1.27 mAh which is consistent with the data shown in Figure 19.

A set of core USABC tests were performed as follows:

- Constant Current Discharge Test
- HPPC Test
- 48 hour Stand Test

3 cells were selected to perform cycle life tests at C rate down to 80% rated capacity. An additional 3 cells were selected to perform calendar life tests at 100% state of charge (SOC). The testing was completed at an upper operating voltage of 4.6 V and temperature of 30 C.

The cycle life testing data is shown in Figure 31. The capacity and resistance as a function of cycle number are shown in the top and bottom panels, respectively. The cells completed 80 cycles down to an 80% capacity retention cutoff at 4.6 V most likely due to high resistance change between 50 and 100 cycles. Cells were shutoff at RPT (Reference Performance Test) 3 (150 cycles).

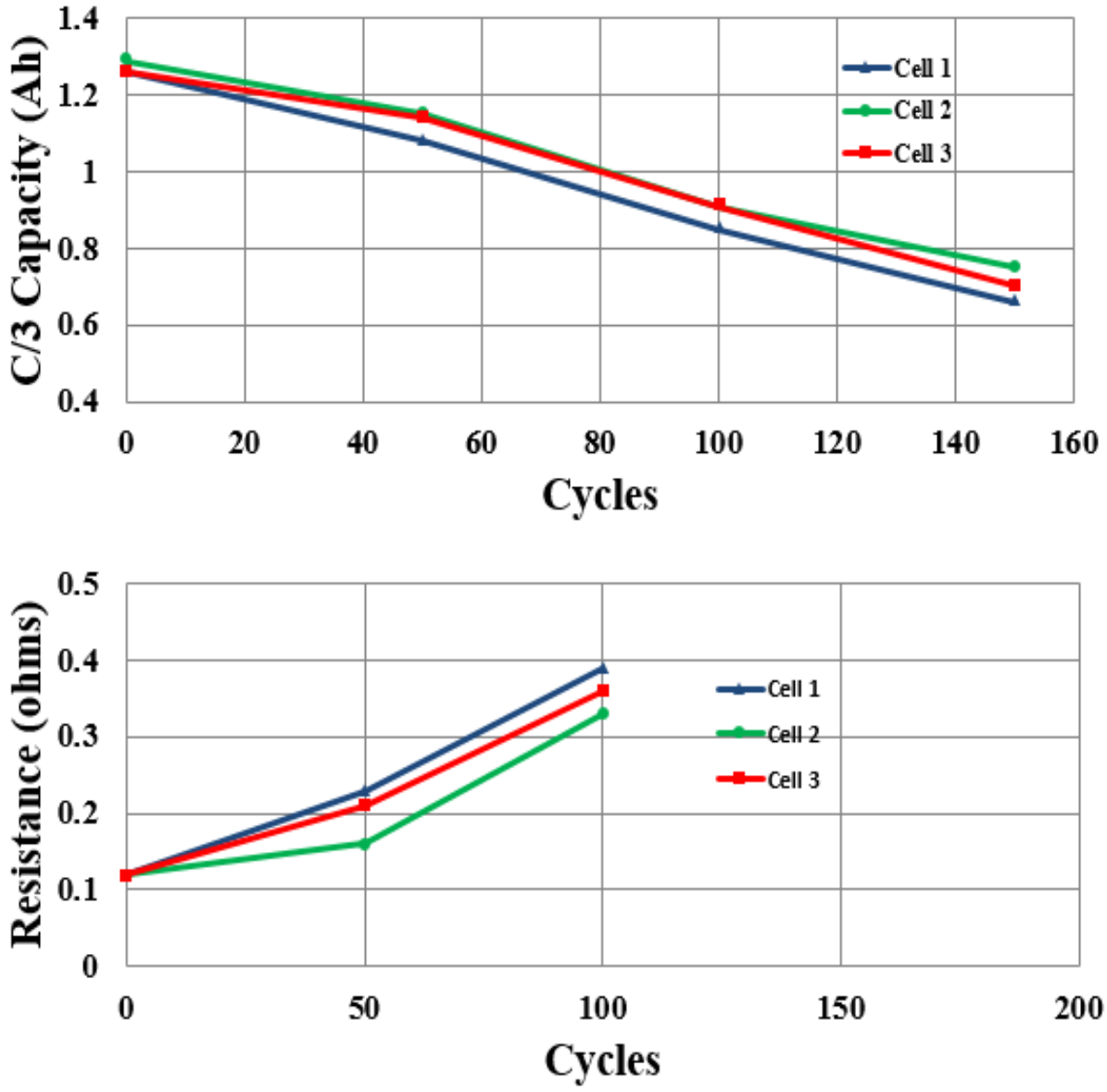

Figure 31 Cycle life capacity (top) and resistance data for Daikin best practice electrolyte at 4.6 V

The calendar life test is shown in Figure 32. The calendar life did not finish RPT6. The drop in capacity in the 10th week is again consistent with a large resistance increase. The cause of the resistance has not been determined yet but it is believed it is related to the thickness change in the anode.

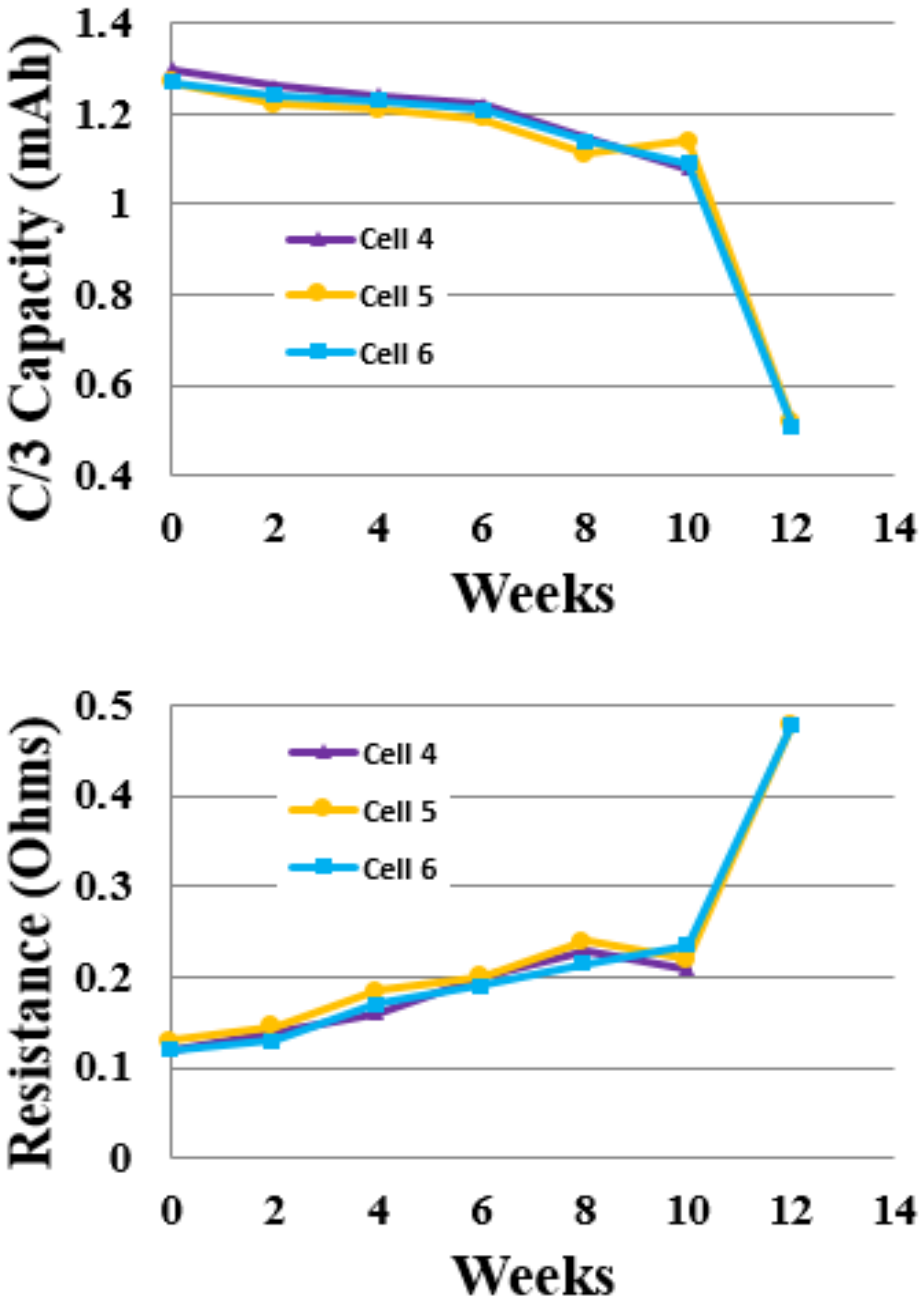

Figure 32 Calendar life capacity (top) and resistance data for Daikin best practice electrolyte at 4.6 V

The minimal target was to reach 300 cycles down to 80% capacity retention when cycled to 4.6 V. The objective was not met for the interim cells. Incremental improvements have been made for the submission of the final cells. Understanding the failure mechanisms at 4.6 V has not been accomplished in the time frame of this project and will be addressed in a new DOE project.

Calendar life and gassing of FEC

Although superior cycling performance above 4.35 was noted for fluorocarbon based electrolytes, calendar tests results show significant gassing in the fluorocarbon electrolytes. Minimal residence time at high voltage is achieved in cycle life experiments. Calendar life experiments were started where the NMC111/graphite cells were CC/CV charged to 4.6 V and allowed to sit at room temperature. The drop in OCV and gas volume were collected over a 600 hour period (see Figure 33). The data shows that the fluorinated electrolyte has a lower OCV drop. This is consistent with it being more stable towards oxidation at the cathode. Conversely, the hydrocarbon electrolyte is easily oxidized by the cathode which results in reduced cathode (i.e. lower voltage). However, the fluorinated electrolyte has high rate of gassing which is opposite of that seen in the cycle life experiments.

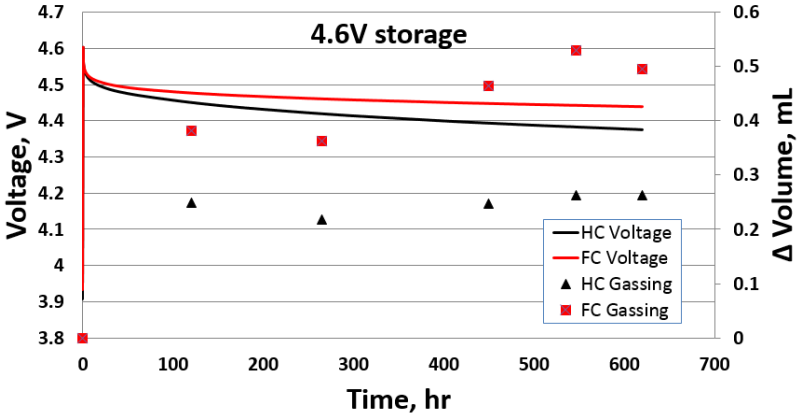

Figure 33 ΔOCV and Δ gas volume over time for NMC111/graphite cells filled with fluorocarbon and hydrocarbon electrolyte

Batteries have been filled with both fluorinated (containing FEC) and conventional electrolyte then were oven aged at 60 C for 72 hours. These batteries were charged from voltages between 4.2 and 4.8 V. The OCV drop and gassing volume were measured after the 72 hours aging (see Figure 34). The data show a clear linear dependence of the decomposition of FEC with voltage. The data again shows that the fluorinated electrolyte is more stable against oxidation at the cathode.

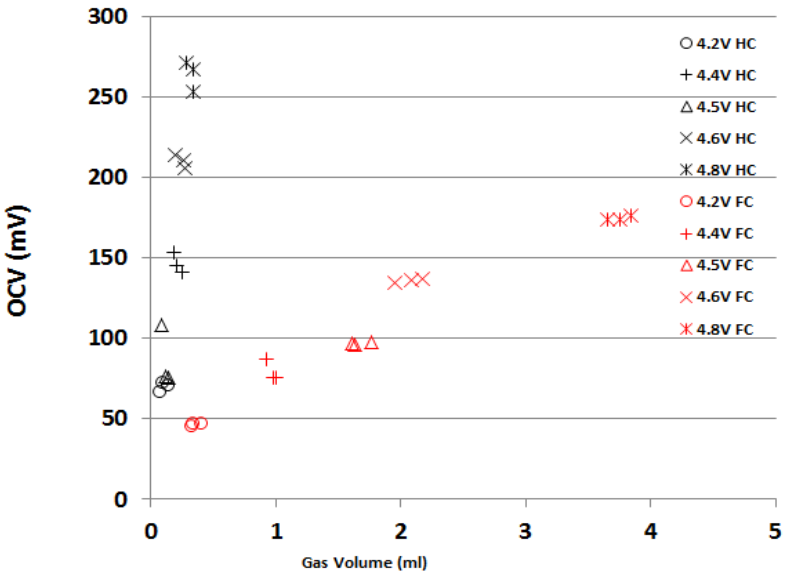

Figure 34 Δ OCV vs. gas volume for fluorocarbon and hydrocarbon electrolyte filled NMC111/graphite cells stored at 60 C for 72 hours at several voltages.

OCV vs. gas volume data has also been collected for a variety of compositions and is shown in Figure 35. There is a

clear dependence of gas volume on the concentration of FEC as it varies from 0 to 50 volume percent. The data also shows the benefit of the mixture with propane sultone (PS) resulting in lower gassing. Finally, the data shows the relationship between gassing and the identity of the organic hydrocarbon carbonate. The gassing hierarchy is diethyl carbonate (DEC) < ethyl methyl carbonate (EMC) < dimethyl carbonate (DMC). The electrolyte conductivity and rate performance shows the opposite trend.

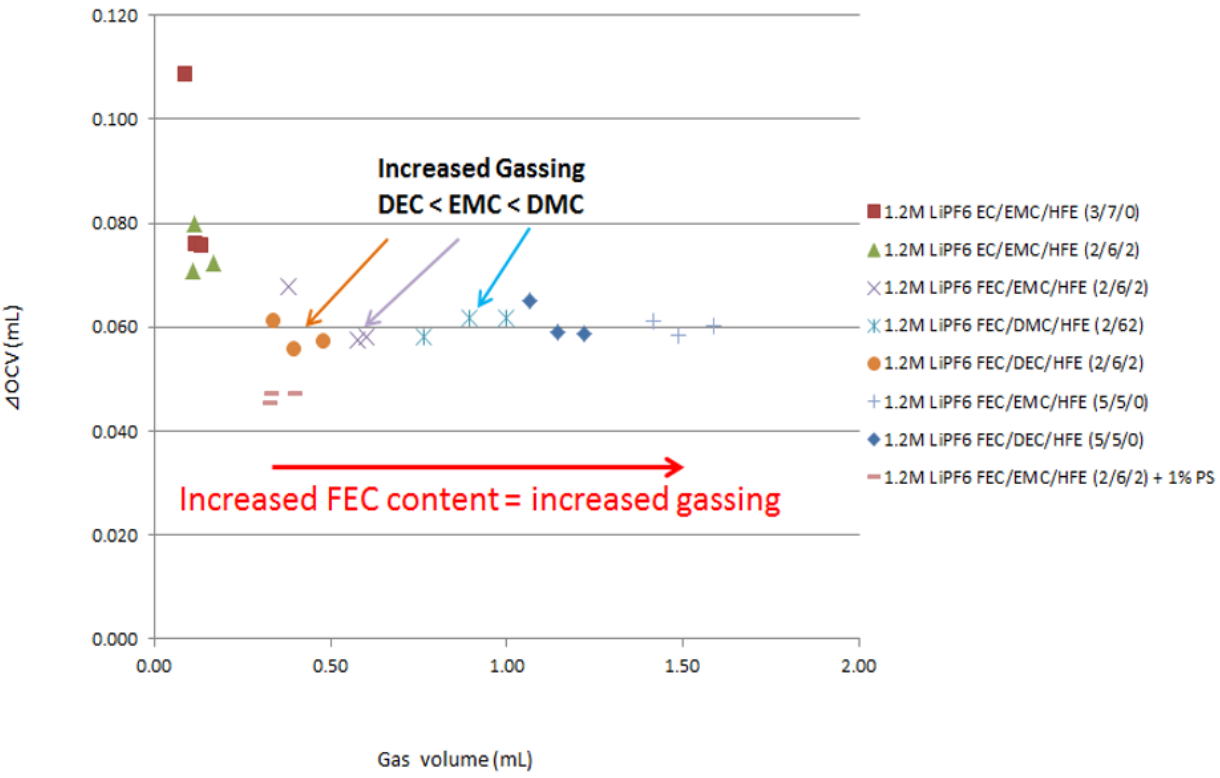

Figure 35 Δ OCV vs. gas volume for NMC111/graphite cells stored at 60 C for 72 hours at 4.5 V. The cells are filled with various compositions of fluorinated electrolyte.

Physical post mortem analysis of electrodes

Preliminary surface studies of the cathode show that the addition of the Daikin fluoroether forms a film on the cathode. Figure 36 shows results of an Auger spectroscopy analysis on charged NMC electrodes from batteries containing several electrolyte compositions containing fluoroether (D7). Figure 36 shows the fluorine molar concentration on the surface against the phosphorus molar concentration. This is done to "remove" the salt anion (PF_6^-) contribution to the fluorine concentration. In all cases, the fluorine: phosphorus ratio is much higher than 6 which is only consistent with fluorine coming from an additional fluorine source. In the two samples to the left, there are two additional sources of fluorine possible FEC and fluoroether (D7). However, the two samples on the left only contain the fluorether (D7) yet still show significant fluorine concentration at the cathode. Figure 37. shows the

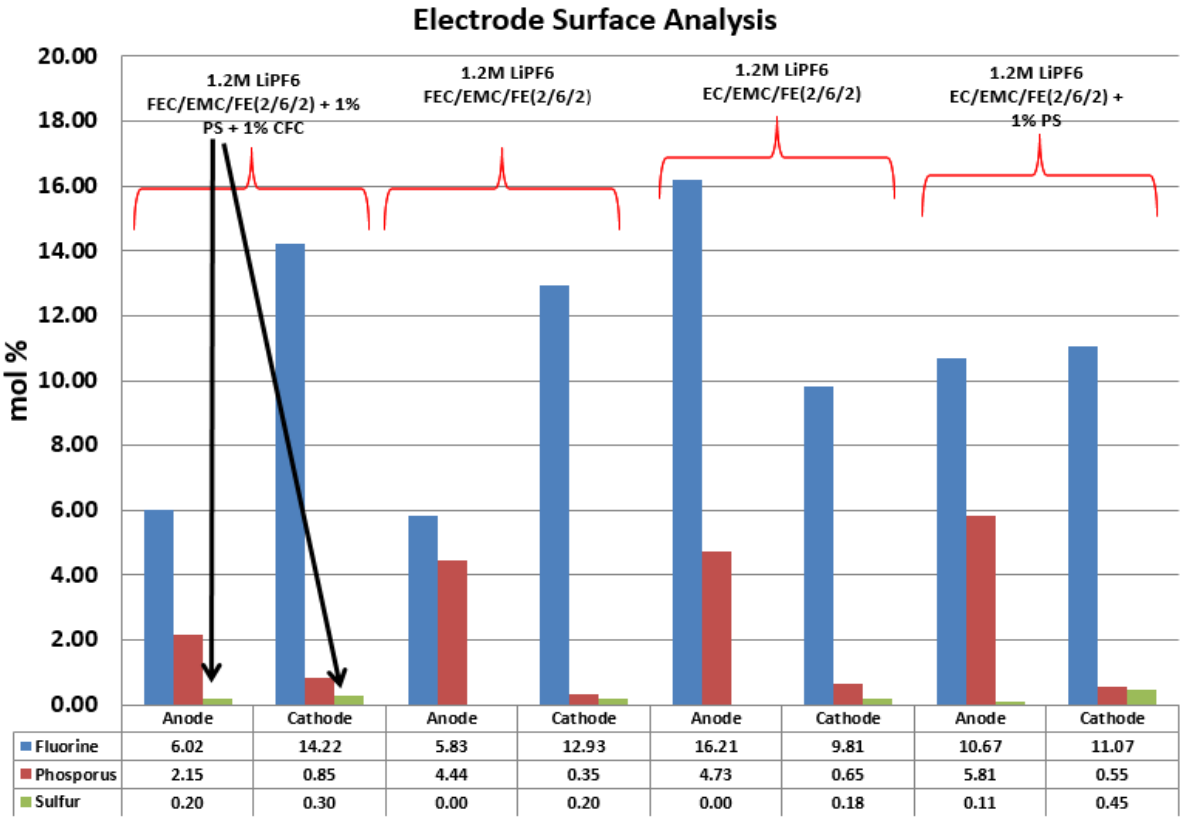

Figure 36 Auger analysis of NMC111/graphite cathode and anode surfaces for four different electrolytes. Fluorine (blue), phosphorus (red) and sulfur (green) concentrations are shown.

fluorine/manganese/nickel concentration at both the surface and down 25 microns. The manganese/nickel concentration is an indication of cathode presence. The fluorine/metal molar ratio is much higher at the surface and flips at 25 micron which again points to fluorinated film formation. These initial experiments are done only for cathodes and anodes which are charged to 4.5 V. The surface analysis has not yet been completed for cells charged to 4.6 V. The cells sent to Argonne which were tested at 4.6 V did not pass either the cycle or calendar life test. The first thing noted on the returned cells was the thickness change in the discharged cells. Parallel cycling tests were completed at Daikin. Figure 38 shows side

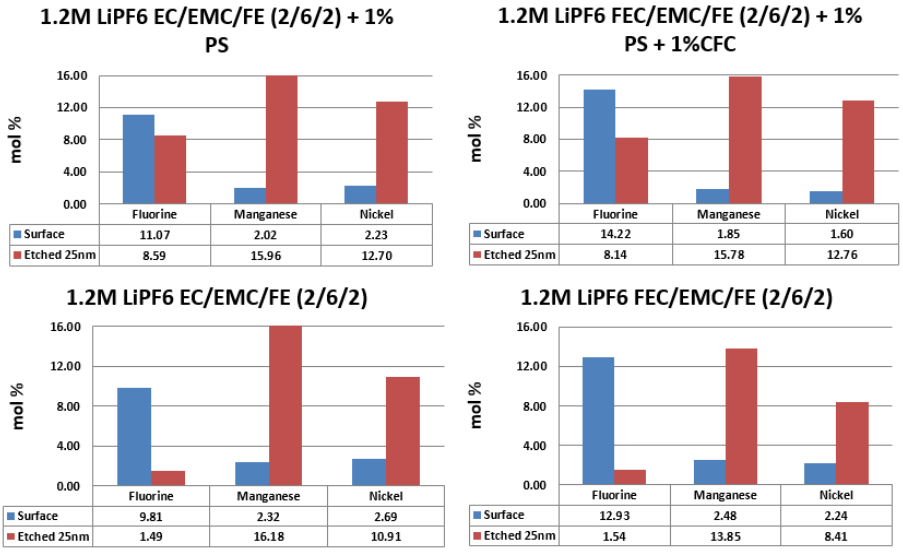

Figure 37 Auger depth analysis showing the fluorine, manganese, and nickel content at the surface of and 25 nm into the cathode surface for 4 different electrolytes

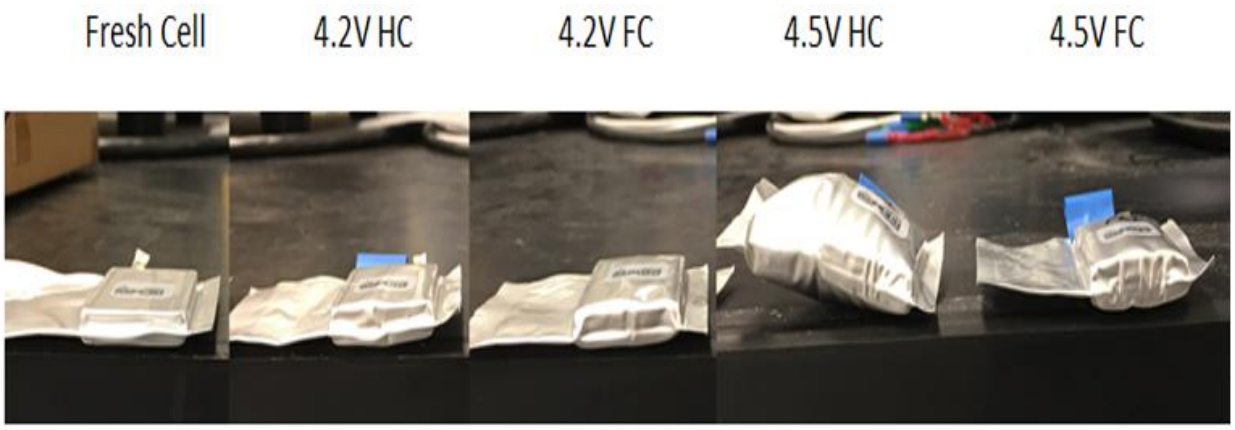

Figure 3Photographs of NMC111/graphite cells filled with hydrocarbon electrolyte and fluorocarbon electrolyte (fresh, post cycling 4.2 and 4.5 V)

profile view photographs from left to right of fresh (dry-no electrolyte), cells discharged at 4.2 V, and cells discharged at 4.5 V. There are two types of volume change noted in the cell which come from gassing and electrode swelling. Gassing can be noted readily in both cells containing conventional hydrocarbon (HC) electrolyte particularly the cell discharged at 4.5 V. It has been shown by Daikin that the source of the gassing is from the interaction of the hydrocarbon electrolyte with the highly oxidized NMC cathode. The fluorosolvent which Daikin uses as an additive has been shown to mask the cathode and minimize the gas generation which is what is observed for the fluorocarbon electrolyte (FC) cell cycled at 4.5 V (Figure 38 right panel. However, the cell still experiences a large amount of non-gas swelling due to the electrodes.

Table III. Tabulated thickness values of the cell, anode and cathode from the cells shown in Figure 38

	Overall Thickness (in)	Cathode Thickness (in)	Anode Thickness (in)	Cathode/Anode Layers
Empty Cell	0.220	0.006	0.006	15
4.2V HC	0.296	0.007	0.011	15
4.2V FC	0.278	0.006	0.010	15
4.5V HC	0.490	0.008	0.022	15
4.5V FC	0.443	0.007	0.019	15

Table III shows the thickness of the cells in Figure 38 and the thicknesses of the individual electrodes. It can be seen clearly that the primary contributor to the cell swelling is the anode. The source of the anode thickness change is not yet understood. Daikin is working on elemental, thermal and structural analysis of these electrodes. Although the fluorosolvent was

shown to make a film on the cathode, it appears that the film growth is not progressive and has little overall effect on the cathode thickness. On closer inspection, there is significant damage to the anode extracted from the 4.5 V cycled cell which contained conventional (HC) electrolyte. This damage results in a delaminated electrode. This is not observed for the anode from the 4.5 V fluorocarbon electrolyte filled cell. It is hypothesized that this damage is caused by the gas generation although it is not clear why it is happening at the anode. Figure 39 shows the anode and cathodes extracted from both cells. There is no visible damage or delamination to the cathode in either case.

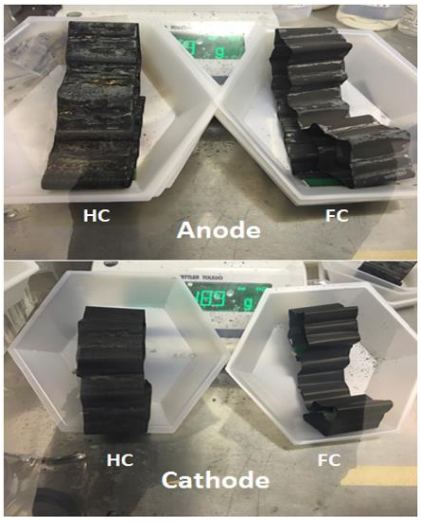

Figure 4 Photos of anode and cathode extracted from NMC111/graphite cells cycled at 4.5 V. Thicknesses shown in Table III.

Thermal analysis of the charged anodes has been initiated to determine chemical/physical nature of the dimension change of the electrodes. Figure 40 shows the differential scanning calorimetry (DSC) and thermal gravimetric analysis (TGA) traces of anodes taken from cells cycled at 4.2 and 4.5 V. The DSC traces for the hydrocarbon (black) cells both show a thermal event beginning below 100 C. For the high voltage (4.5 V) cell, this coincides with a large weight loss. It is hypothesized that in the electrodes swollen at high voltage that solvent is physically occluded in the electrode. This occlusion is less pronounced in fluorocarbon electrolytes either due to wetting (viscosity) or chemical differences. The DSC trace (red dashed) for the 4.5 V FC anode also shows a thermal event consistent with the small weight loss (less occlusion). Both (HC and FC) 4.2 V anodes show weight gain in the TGA traces. This is attributed to remnant lithium metal forming hydroxide then

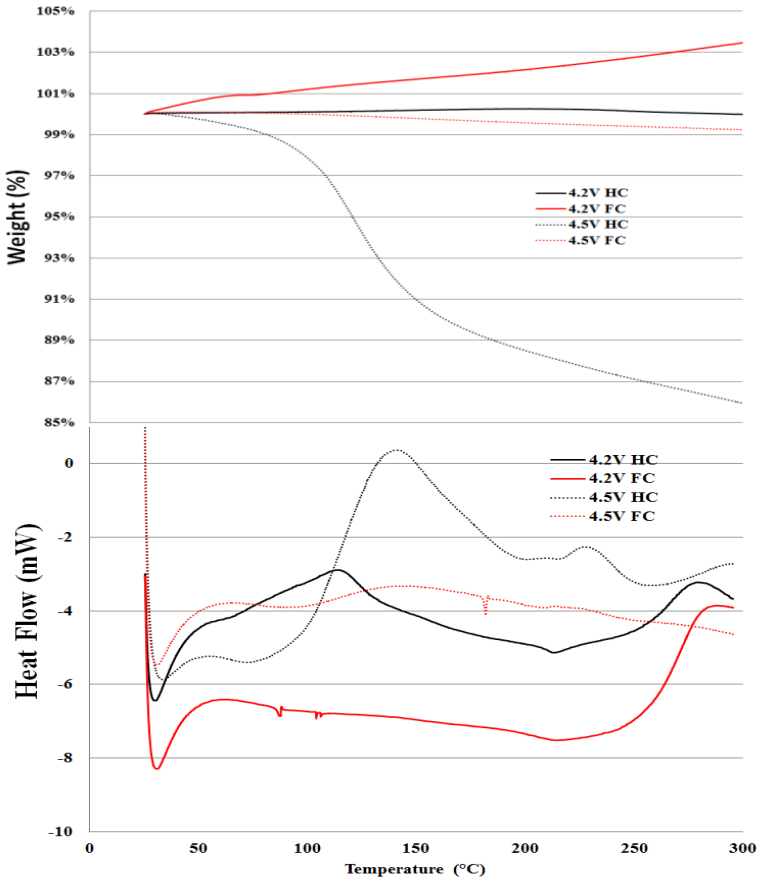

Figure 40 Thermogravimetric (TGA) and calorimetric (DSC) data for the anodes taken from cells containing fluorocarbon (FC) and hydrocarbon (HC) after cycling at 4.2 and 4.5 V

carbonate. A more complete understanding of the thermal behavior needs to be complete including analysis of the evolved gas.

Safety performance

Generally, fluorinated solvents tend to have higher flashpoints than their hydrocarbon analogs which is primarily due to higher viscosity and lower vapor pressure. Table IV. shows the flashpoints of several common lithium ion electrolyte solvents as compared to fluoroether (FE). In general, fluorocarbons exhibit higher flash points than hydrocarbons.

Table IV Flashpoints of common electrolyte solvents compared to the fluoroether

	FP(℃)
EC	150
FEC	129
DMC	14
EMC	23
DEC	33
FE	No

The key understanding to battery safety in lithium ion batteries is to understand the interaction of a flammable electrolyte, a highly oxidized electrode (cathode) and an ignition source (heat, spark). The triangle of fuel, oxididant, and source needs to be interrupted to impart safer operation of lithium ion batteries. Engineering solutions like overcharge protection circuits and fire containment can be implemented to isolate/remove the ignition sourece. Moving to a less oxidizing cathode (ie. $LiFePO_4$) generally means less overall energy in the resulting battery and fire hazard still exists due to the electrolyte. The

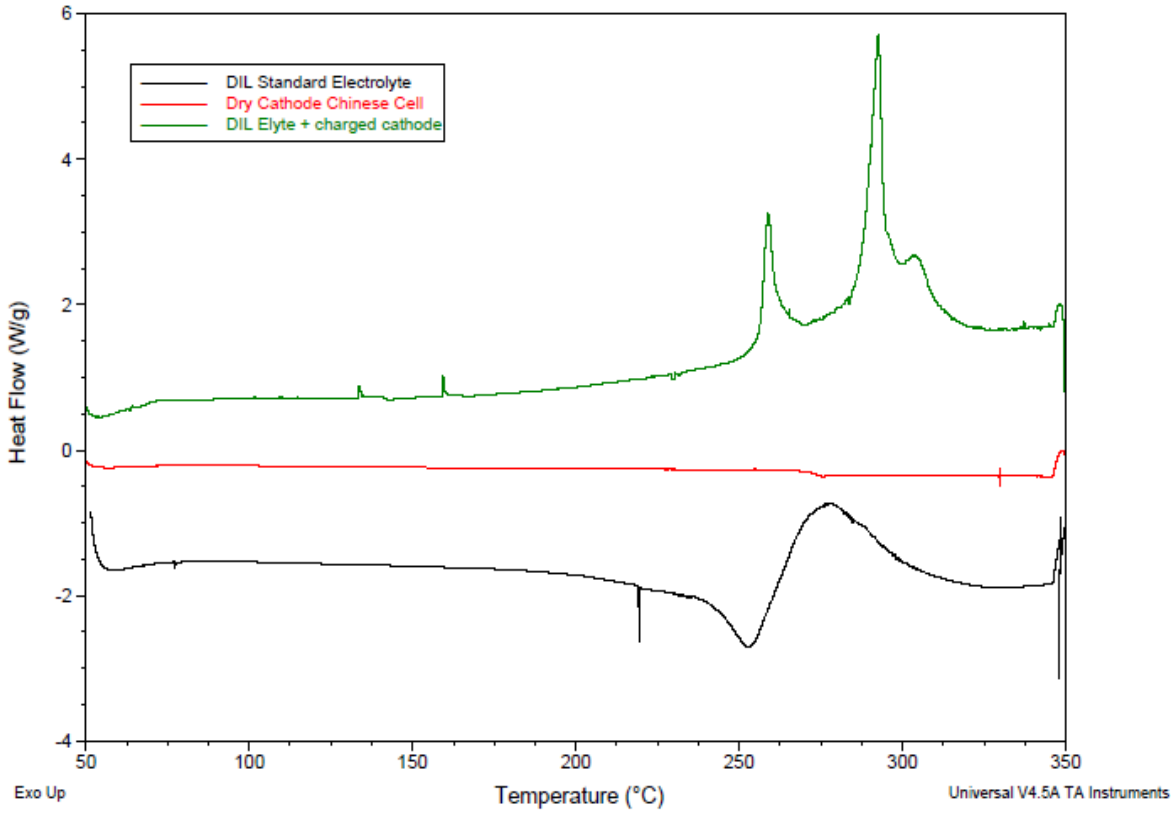

Figure 41 Differential scanning calorimetry traces showing 1) electrolyte only (bottom) 2) dry cathode only (middle) and 3) electrolyte with charged cathode (top)

possibility of fire is best removed by lowering/eliminating flammable electrolyte. This can be done by substitution of the current flammable hydrocarbons with high/no flashpoint fluorocarbons.

Differential scanning calorimetry was used to examine the interaction of the electrolyte with charged electrode surfaces. NMC111/graphite cells were charged to 4.5 V and carefully disassembled without shorting the cells. The electrode coatings were scraped off while wet with electrolyte and placed into high pressure calorimetry pans. The first DSC experiment completed with standard hydrocarbon electrolyte is shown in Figure 41. This experiment shows the neat electrolyte (bottom) and the dry cathode (middle) compared to the mixture of the charged cathode (NMC111) with the electrolyte. The sample with the charged cathode shows multiple exothermic events above 250 C.

A second calorimetry experiment showing the reaction difference between fluorocarbon and hydrocarbon based electrolytes is shown in Figure 42. The figure shows the DSC data for hydrocarbon (bottom trace), fluorocarbon (middle trace) and mixed 60% hydrocarbon/40% fluorocarbon electrolyte in the presence of a charged NMC111 cathode. The exotherms for the samples containing fluorocarbon electrolytes are pushed to higher temperatures and are broadened. The broadening of the exotherm means that the heat buildup is more gradual and a greater chance of heat dissipation is achieved.

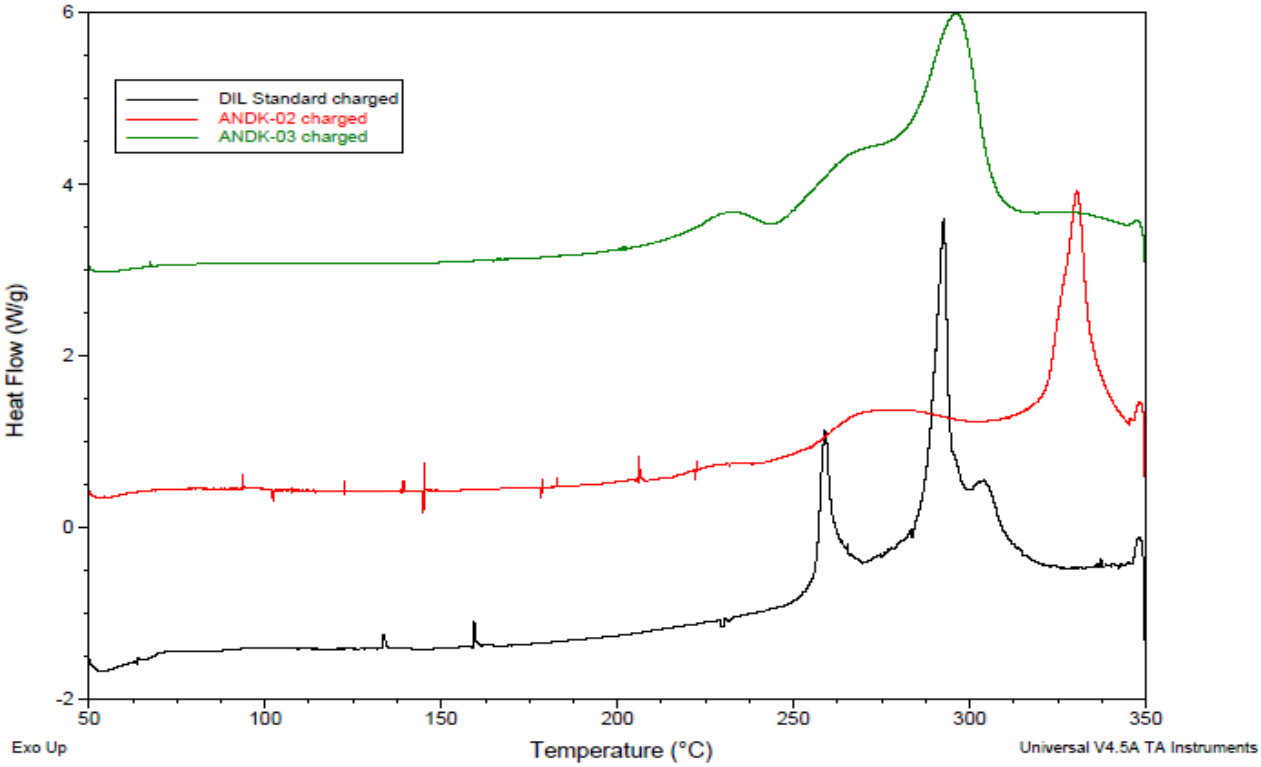

Figure 542 DSC data for hydrocarbon (bottom), fluorocarbon, and 60/40 hydrocarbon/fluorocarbon electrolyte in presence of charged NMC111 cathode

In practice, this can be demonstrated in abuse testing. Abuse testing (overcharge, nail penetration) has been performed on the Daikin fluorinated electrolyte vs. the hydrocarbon control. The testing has been performed on several chemistries including LCO, NMC111, NCA and NMC532. In all cases, Daikin fluorinated electrolyte performs significantly better than the hydrocarbon control. An example of this can be seen in the photos in Figure 43. The photos show an overcharge test on NMC111/graphite cells. The cells filled with hydrocarbon control electrolyte and Daikin fluorinated electrolyte are on the left and right, respectively. The overcharge was to 18 V and the charging current used was 2C. The top left panel shows the

Figure 43 Photos of cells containing hydrocarbon (left) and fluorocarbon (right) electrolyte at 10, 1400, and 1500 seconds overcharging.

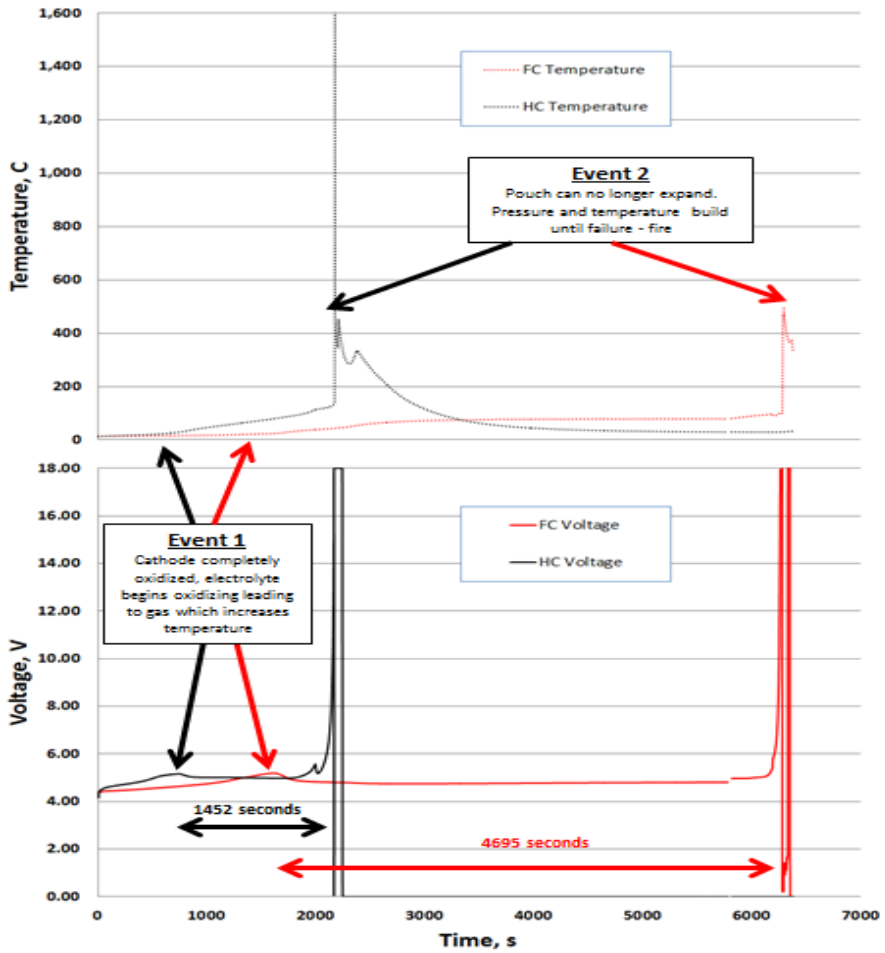

Figure 44 Voltage and temperature data for both cells shown in previous figure photo.

beginning of the test, the middle panel (1400 seconds) shows significant gassing in the hydrocarbon cell and eventually the hydrocarbon cell catches fire. Both voltage and temperature data are collected on both cells. Temperature is collected by a thermocouple affixed directly to the cell. As can be seen in Figure 44., the voltage reaches a maximum when the cathode is delithiated (arrows). After this point, input of additional energy causes the electrolyte to decompose to gas. The resulting pressure increase in the pouch cell causes a temperature increase until the cell eventually ignites. It takes 1452 seconds for the hydrocarbon cell to ignite while it takes 4650 seconds for the Daikin electrolyte to ignite. It should be noted that the Daikin electrolyte still has 60% hydrocarbon (EMC) present.

Conclusions

In fulfillment of DOE funding opportunity, construction and preliminary evaluation of cells to be submitted to the DOE has been completed. This is to fulfill milestone of the funded project. 3 groups of 10 cells each have been assembled. The cells are NMC111/graphite 1 Ah pouch cells which contain either hydrocarbon (10 cells) or fluorocarbon electrolyte. The fluorocarbon electrolyte is current Daikin best practice electrolyte. The cells have been formed at the voltages which are suggested for testing. 10 cells containing hydrocarbon electrolyte and 10 containing fluorinated Daikin best practice electrolyte were formed at 4.5V. 10 cells containing the fluorinated electrolyte were formed at 4.6V. A test plan is being developed for these cells to show that the failure point of fluorinated electrolyte occurs between 4.5 and 4.6V.

1. 10 cells of control electrolyte 1.2M $LiPF_6$ EC/EMC (2/8) + 1% PS to test at 4.5 V
2. 10 cells of best guess fluorinated electrolyte 1.2M $LiPF_6$ FEC/EMC/D7 (2/6/2) + 1% PS + 1% W9 to test at 4.5 V
3. 10 cells of best guess fluorinated electrolyte 1.2M $LiPF_6$ FEC/EMC/D7 (2/6/2) + 1% PS + 1% W9 to test at 4.6 V

To allow best optimal performance, after formation the cells were stored at room temperature to allow best possible wetting of the electrodes. It was also done to make sure the fabricated cells were stable. The cells have been charged to a nominal voltage of 3.4 V for shipping. Figure 45 shows the voltage measured after a month of storage is very stable and the samples were shipped

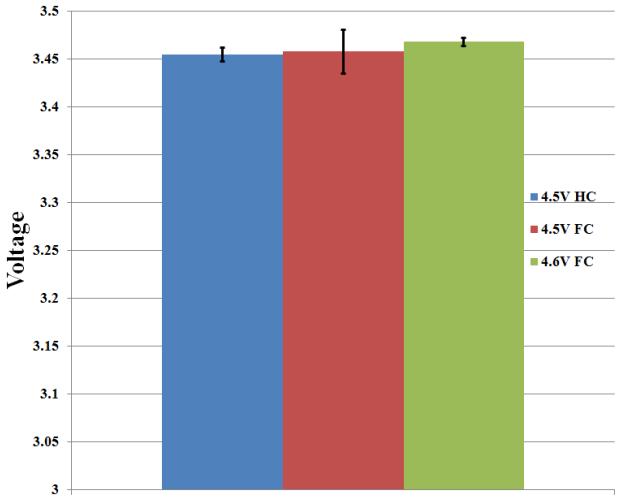

Figure 45 1 month OCV data for NMC111/graphite cells stored at RT and charged to 3.4 V shipping charge.

Daikin has acquired an extensive knowledge of the performance of fluorochemicals as solvents/additives in lithium ion electrolytes. In general, the advantage of using a fluorocarbon based electrolyte is best realized for batteries which require high voltage, high temperature and/or safer operation. In this study, Daikin has demonstrated the following:

1. Significant energy gains can be realized by operating existing lithium ion chemistries at elevated voltage (> 4.35 C)
2. Batteries which contain conventional state of the art hydrocarbon electrolytes are unable to cycle at these elevated voltages. The primary failure mechanism for these batteries is gassing due to the electrochemical breakdown of the electrolyte at/near 4.35 V.
3. By substituting fluorocarbons for hydrocarbons in conventional electrolytes, batteries are able to cycle well above the 4.35 decomposition voltage. The current performance limit with best practice fluorocarbon electrolyte is between 4.5 and 4.6 V
4. Special care needs to be taken in the formulation of fluorocarbon electrolytes. Fluoroethylene carbonate (FEC) exhibits gassing due to breakdown at higher voltage. This has significant implications in the implementation of silicon anodes in high performance batteries. To date, successful operation of silicon anodes has not been shown without FEC in the electrolyte.
5. Daikin fluoroethers form a film on the cathode in NMC/graphite cells. The film is primarily fluorochemical in nature and is less than 25 microns thick. It is hypothesized that the film formation is a factor in high voltage operation by masking the highly oxidized surface of the cathode from the electrolyte forestalling breakdown.
6. There is considerable swelling (non-gas) of the electrodes in the NMC/graphite batteries when cycled above 4.5 V.

Acknowledgment: "This material is based upon work supported by the Department of Energy under Award Numbers **DE-EE0-006437**."

References

1) Armand, M. and J. M. Tarascon. "Building Better Batteries", *Nature*, **2008**, *451*, 652.

2) R. Maron, S. F. Amalraj, N. Leifer, D. Jacob, and D. Aurbach, "A review of advanced and practical lithium battery materials", *J. of Materials Chemistry*, **2011**, *21*, 9938-9954.

3) B. Michalak, H. Sommer, D. Mannes, A. Kaestner, T. Brezesinksi, and J. Janek, "Gas Evolution in Operating Lithium-Ion Batteries Studied In-Situ by Neutron Imaging", *Scientific Reports*, **2015**, *5*, Pub No. 15627.

4) Nitta, Naoki, F. Wu, J. T. Lee, and G. Yushin, "Li-ion battery materials: present and future", *Materials Today*, **2015**, *18*, 252-264.

5) Aurbach, Doron, B. Markovsky, G. Salitra, E. Markevich, Y. Talyossef, M. Koltypin, L. Nazar, B. Ellis, and D. Kovacheva. Review on electrode–electrolyte solution interactions, related to cathode materials for Li-ion batteries. *J. Power Sources*, **2007**, *165*, 491–499.

6) Berkes, B.B., A. Jozwiuk, M. Vracar, H. Sommer, T. Brezesinski, and J. Janek. Online continuous flow differential electrochemical mass spectrometry precision, long-term cycling tests. *Anal. Chem.*, **2015**, *87*, 5878–5883.

7) Onuki, Masamichi,, S. Kinoshitaa, Y. Sakataa, M. Yanagidatea, Y. Otakea, M. Uea, and M. Deguchib. "Identification of the source of evolved gas in Li-ion batteries using 13C-labeled solvents". *J. Electrochem. Soc.*, **2008**, *155*, A794–A797.

8) Self, Julian, C. P. Aiken, Remi Petibon, and J. R. Dahn. "Survey of Gas Expansion in Li-Ion NMC Pouch Cells", *J. Electrochem. Soc.*, **2015**, *162*, A796–A802.

9) Aurbach, Doron, Y. Ein-Eli, O. Chusid, Y. Carmeli, M. Babai, and H. Yamin. "The Correlation Between the Surface Chemistry and the Performance of Li-Carbon Intercalation Anodes for Rechargeable 'Rocking-Chair' Type Batteries", *J. Electrochem. Soc.*, **1994**, *141*, 603.

10) Aurbach, Doron. Review of selected electrode-solution interactions which determine the performance of Li and Li ion batteries, *J. Power Sources*, **1999**, *89*, 206.

11) Ouatani, L. E., R. Dedryvere, C. Siret, P. Biensan, S. Reynaud, P. Iratcabal, and D. Gonbeau, "The Effect of Vinylene Carbonate Additive on Surface Film Formation on Both Electrodes in Li-Ion Batteries", *J. Electrochem. Soc.*, **2009**, *156*, A103.

12) Broussely, Michel, M, P. Biensan, F. Bonhomme, P. Blanchard, S. Herreyre, K. Nechev, and R. J. Staniewicz. "Main aging mechanisms in Li ion batteries", *J. Power Sources*, **2005**, *146*, 90-96.

13) Andrzej Lewandowski, , Agnieszka Świderska-Mocek "Ionic liquids as electrolytes for Li-ion batteries—An overview of electrochemical studies" *J. Power Sources*, **2009**, *194*, Pages 601–609.

14) M. Jacoby, "Assessing the Safety of Lithium-Ion Batteries", *C & EN*, **2013,** *91*, 33-37.

15) For a comprehensive review see *Fluorinated Materials for Energy Conversion;* Tsuyoshi Nakajima and Henri Groult, Eds. Elsevier Books, **2005.**

16) Nishikawa, Daiki, T. Nakajima, Y. Ohzawa, M. Koh, A. Yamauchi, M. Kagawa, and H. Aoyama. "Thermal and oxidation stability of organo-fluorine compound-mixed electrolyte solutions for lithium ion batteries" *J. Power Sources*, **2013**, *243*, 573-580.

17) Ohmi, Naoki, T. Nakajima, Y. Ohzawa, M. Koh, A. Yamauchi, M. Kagawa, and H. Aoyama. "Effect of organo-fluorine compounds on the thermal stability and electrochemical properties of electrolyte solutions for lithium-ion batteries" *J. Power Sources*, **2013**, *221*, 6-13.

18) Matsuda, Yuki, T. Nakajima, Y. Ohzawa, M. Koh, A. Yamauchi, M. Kagawa, and H. Aoyama. "Safety improvement of lithium ion batteries by organo-fluorine compounds" J. *Fluorine Chemistry*, **2011**, *132*, 1174-1181.

19) Achiha, Takashi, T. Nakajima, Y. Ohzawa, M. Koh, A. Yamauchi, M. Kagawa, and H. Aoyama. "Thermal stability and electrochemical properties of fluorine compounds as nonflammable solvents for lithium-ion batteries", *J. Electrochem. Soc*., **2010**, *157(6)*, A707-A712.

20) Achiha, Takashi, T. Nakajima, Y. Ohzawa, M. Koh, A. Yamauchi, M. Kagawa, and H. Aoyama. "Electrochemical Behavior of Nonflammable Organo-Fluorine Compounds for Lithium Ion Batteries", *J. Electrochem. Soc*., **2009** *156(6)*, A483-A488.

21) Koh, Meiten, A. Yamauchi, Y. Takagawara, and H. Aoyama. "Synthesis and electrochemical properties of the fluorinated polymer electrolytes", Abstracts of Papers, 230th ACS National Meeting, Washington, DC, United States, Aug. 28-Sept. 1, **2005** (2005), POLY-574.

22) Kim, J-H, N. P. W. Pieczonka, Z. Li, Y. Wu, S. Harris, and B.R. Powell. Understanding the capacity fading mechanism in $LiNi_{0.5}Mn_{1.5}O_4$/graphite Li-ion batteries. *Electrochim. Acta*, **2013**, *90*, 556–562.

23) Yang, Li, B. Ravdel, and B. L. Lucht. Electrolyte reactions with the surface of high voltage $LiNi_{0.5}Mn_{1.5}O_4$ cathodes for lithium-ion batteries. *Electrochem. Solid-State Lett.*, **2010**, *13*, A95-A97.

24) Pieczonka, Nicholas P.W., Z. Liu, P. Lu, K. L. Olson, J. Moote, B. R. Powell, and J-H. Kim. Understanding transition-metal dissolution behavior in $LiNi_{0.5}Mn_{1.5}O_4$ high-voltage spinel for lithium ion batteries. *J. Phys. Chem.,* **2013,** *C 117,* 15947–15957.

25) Zhengcheng Zhang, Libo Hu, Huiming Wu, Wei Weng, Meiten Koh, Paul C. Redfern, Larry A. Curtiss and Khalil Amine "Fluorinated electrolytes for 5 V lithium-ion battery chemistry" *Energy Environ. Sci.*, **2013**, *6*, 1806-1810.

26) Sinha, N. N., A. J. Smith, J. C. Burns, G. Jain, K. W. Eberman, E. Scott, J. P. Gardner, and J. R. Dahn. "The Use of Elevated Temperature Storage Experiments to Learn about Parasitic Reactions in Wound $LiCoO_2$/Graphite Cells", *J. Electrochem. Soc.,* **2011**, *158*, A1194-A1201

27) A. J. Smith, J. C. Burns, S. Trussler and J. R. Dahn, "Precision Measurements of the Coulombic Efficiency of Lithium-Ion Batteries and of Electrode Materials for Lithium-Ion Batteries", *J. Electrochem. Soc.,* **2010**, *157*, A196-A202.

28) A. J. Smith, J. C. Burns, and J. R. Dahn, "A High Precision Study of the Coulombic Efficiency of Li-Ion Batteries, *Electrochem. Solid-State Lett.,* **2010**, *13*, A177-A179.

29) J. C. Burns, G. Jain, A. J. Smith, K. W. Eberman, E. Scott, J. P. Gardner, and J. R. Dahn, "Evaluation of Effects of Additives in Wound Li-Ion Cells Through High Precision Coulometry", *J. Electrochem. Soc.,* **2011**, *158*, A255-A261.

30) A. J. Smith, and J. R. Dahn, "Delta Differential Capacity Analysis", *J. Electrochem. Soc*., **2012**, *159*, A290-A293.

31) Christopher L. Campion, Wentao Li, and Brett Lucht, "Thermal Decomposition of $LiPF_6$-based Electrolytes for Lithium-Ion Batteries", *J. Electrochem Soc,* **2005**, *152 (12),* A2327-A2334.